DEL HORNO, L., SEGURA, E., MORALES, R. y SOMOLINOS, J.A., 2020. Exhaustive closed loop behavior of an one degree of freedom first-generation device for harnessing energy from marine currents. Applied energy, vol. 276, ISSN 0306-2619. DOI 10.1016/j.apenergy.2020.115457.

Exhaustive Closed Loop Behavior of an One Degree of Freedom First-Generation Device for Harnessing Energy from Marine Currents

L. del Horno[a], E. Segura[a,b], R. Morales[a,b,*], J.A. Somolinos[a]

[a] *Grupo de Investigación Tecnológico en Energías Renovables Marinas (GIT-ERM), E.T.S Ingenieros Navales, Universidad Politécnica de Madrid, Arco de la Victoria 4, 28040, Madrid, Spain.*
[b] *E.T.S. Ingenieros Industriales, Universidad de Castilla-La Mancha, Campus Universitario, Avda. Spain s/n, 02071, Albacete, Spain.*

Abstract

The use of ballast systems to carry out automatic emersion/immersion maneuvers for first generation tidal energy converters (TECs) has aroused the interest of researchers and technicians as new technique by which lower installation and operation and maintenance (O&M) costs (a reduction of the installation costs by 10% and O&M by 15%). Very simple dynamic models have been obtained and subsequently employed in order to propose various control schemes with which to carry out this sort of maneuvers in devices with different degrees of freedom. This paper provides a detailed study of the closed loop behavior of a gravity-based first generation TEC, which performs only vertical movements with a single degree of freedom. The dynamic behavior of the set (system + controller) is analyzed when the parameters, obtained from its nominal dynamic model and used to design the controller, cannot correspond faithfully with the real parameters of the system. The effects of large uncertainties on the rigid body and the influence on the viscous terms of the added masses of the device are analyzed. The effect of strong additive disturbances owing to external forces or non-perfect null buoyancy during the performance of emersion/immersion maneuvers is also studied. The effectiveness of the proposed control system and its excellent behavior, even under non-nominal conditions and in the presence of strong external disturbances, together with the performance of the proposed emersion/immersion strategy has been demonstrated by means of numerical simulations and experimental trials on a laboratory prototype. A very simple criterion for the design of controllers is also proposed.

Keywords:
Renewable Energy, Tidal Energy Converters, Cost Reductions, Closed-Loop System, Emersion/Immersion Maneuvers.

*Corresponding author
Email address: rafael.morales@uclm.es (R. Morales)

Nomenclature

$z(t)$	Depth of the geometric center of the cylinder, which is time-dependent.
$z_{ref}(t)$	Reference signal of the desired depth.
$\dot{z}_0$	Speed at the equilibrium point.
$f_1(t)$	Weight force.
$f_2(t)$	Buoyancy force, which is time-dependent.
m	Mass of the body.
$m_{Add}[z(t)]$	Added mass of the body. We propose that this is considered as only a function of the depth, z, ignoring its dependence on the speed, as usually occurs.
$V(t)$	Submerged volume, because actuators will undergo variations in volume, which is considered time-dependent.
V_0	Nominal volume of the body outside the sea[1], which it is considered constant.
$\Delta V_u(t)$	Control volume, actuated by means of a motor reduction gear-spindle and a set of linear pistons.
$V_{Buoy}[z(t)]$	Non-submerged volume of the cylinder, which depends only on the depth, z.
$\Delta V(t)$	Volume Disturbance. These disturbances are a consequence of the external forces $\Delta F(t)$.
$\Delta V_D(t), \widehat{\Delta V}_D(t)$	Additive disturbances. This disturbance corresponds to the sum of all disturbances.
ν	Viscous friction coefficient when it is considered that the friction force is proportional to the square of the speed and opposite motion.
g	Gravity constant.
R	Radius of the cylinder.
γ	Cylinder compressibility coefficient, which is considered constant and positive and is computed only for negative values of depth, z (zero when $z \geq R$).
$\rho_w(z, \theta, \text{Sal})$	Water density, which is considered constant and not as a function of the depth, z, temperature, θ, or salinity, Sal.
ΔT_{EM}	This parameter corresponds to the time taken by the device during the emersion maneuvers.
ΔT_{St}	This parameter is similar to the previous one, but is employed for the immersion maneuvers required for the stabilization of the device at a depth close to the surface.
$\Delta T_{waiting}$	The extra time, which is used for the stabilization of the device and can be as long as desired.
$\widehat{\mathbf{K}}_{F0}, \mathbf{K}_{F0}$	Gain matrix of the state feedback controller.
$\square_0$	Parameters with sub-index $_0$, which are constants with the nominal values considered.
$\square_e$	Parameters with sub-index $_e$, which are estimated values.

Table 1: Nomenclature.

1. Introduction

There is currently great interest in ensuring a sustainable energy supply owing to the limited life span of fossil resources and the serious environmental repercussions that their exploitation has caused [1, 2, 3]. This is the main reason why there has been an international movement to reduce reliance on fossil fuels and place a greater emphasis on the promotion of renewable technologies for electricity generation in order to reduce greenhouse gas emissions, which are responsible for climate change [4, 5, 6, 7]. The European Union (EU) has established the need to achieve a reduction in greenhouse gas emissions of just above 80% with the objective of ensuring that more 80% than of the UE's electricity will be produced by renewable energy sources by 2050 [8]. Several viable renewable energies could be exploited in order to achieve this objective, among which the development of marine technologies is of growing interest [9, 10, 11, 12].

[1] Without compression effects.

If the oceans are considered to be the largest collector, accumulator and transformer of energy on the earth, humanity should view the ocean as one of the most important sources of clean energy [13]. Marine currents, are, together with waves, one of the most promising sources of marine renewable energy (MRE) [14]. The quantification of the energy that could be extracted from sea waves and currents is estimated to exceed 8000 TWh/year [15]. It is expected that the development of the industry for the exploitation of MRE will undergo a significant increase to become in an important source of electricity supply in 2050 [16, 17, 18], by which time it is expected to have an installed capacity of 188 GW of energy originating from oceans [19]. Several technology developers are manufacturing devices that are able to harness tidal/current power in areas with depths lower than 40 meters [20, 21, 22]. These kinds of devices are the so-called first generation TECs (other authors also consider water speed values in order to classify these first generation TECs [23]). The MeyGen Tidal Energy Proyect installed four TECs of this kind with a total capacity of 6 MW and they are located in Pentland Firth (Scotland). In 2018, the project entered its operational phase. Along this year it generated 10 GWh , the equivalent amount of electricity that 2,800 Scottish households consume in one year [24, 25, 26].

In the case of tidal devices employed at depths greater than 40 meters, some authors have proposed the use of different mooring systems and controlled ballast systems in order to execute automatic maneuvers of one degree of freedom (in which only the depth of the device is controlled) [15], two degrees of freedom [27] or even a completely submerged device provided with three degrees of freedom of motion that allow it to move with the possibility of changing the depth and the pitch and yaw angles [28]. A special actuator subsystem has been proposed for this kind of maneuvers [29].

Furthermore, in order to achieve a near future viability of tidal energy and a sustained commercially competitive cost of energy, considerable efforts must be made in order to improve the following factors which influence in the energy production cost [30, 31]: (i) the installation costs can be between 30% and 40% of the capital expenditures (CAPEX) [32]; (ii) the main contribution of the operation expenditures (OPEX) corresponds to maintenance costs [32] and; (iii) the annual energy production (AEP) is linked to the availability of the device (reliability + maintainability). One of the principal keys for the success of MRE is the provision of a secure infrastructure [33] (grid access, supply chain, maintenance service, etc.) by means of the development of new forms of automated and safe installation and maintenance services which allow reducing the aforementioned costs without affecting the energy production. In particular, the proposed work has the objective of developing robust devices for ease-of-installation and ease-of-maintenance operations for gravity-based first generation TECs in order to reduce their installation and maintenance intervals (and consequently their costs) and optimize the harnessing of this energetic resource. The development of these new installation and maintenance services could help to reduce the installation costs by 10% and the operation and maintenance costs by 15% as it has been recently illustrated in [34, 35].

Following this line of research and with the objective to reduce the installation and maintenance costs of gravity-based first generation TECs, this paper deepens into the dynamic behavior of a TEC that is able to emerge to the sea surface and submerge into the operating depth in a safe manner by means of a controlled system of water ballasts and a simple feedback control law. The amount of water in the ballast tanks of the TEC changes its buoyancy and its dynamic behavior, besides there are great uncertainties in the added mass and in the friction term, which are two of the main parameters of its dynamics. This makes necessary to carry out an exhaustive study of the control of these ballast tanks during the evolution of these maneuvers (owing to the fact that emersion and the immersion processes of a first generation TEC are not symmetric in real-life operations and are affected by large disturbances of different nature) in order to achieve a correct and safe functioning of the entire system. This new control system is directly obtained from a very simple dynamic model of an underwater cylindrically shaped device that was experimentally validated in [15]. The study also identifies the effects of the non-nominal parameters of the device under a control system that was tuned using the nominal values of the main parameters of its dynamics. The influence of the variations or non-precise quantification of two main parameters in the controlled system is studied in depth. Firstly, it is well known that the added mass of

an underwater device depends on its relative speed with regard to the fluid, its geometric shape and the surface characteristics of the submerged body, among others. The mass itself of the device can even be altered owing to the presence of bio-fouling or the corrosion of the steel. Secondly, the viscous friction or the drag coefficients are not usually well determined. The main objective of this paper is to present the behavior of a device with two proposed controllers of increased complexity when both are working supposing non-nominal values (mass and friction) and even with large variations in the values of both parameters.

The remainder of the paper is organized as follows: Section 2 resumes the principal characteristics of the manual and automated installation and maintenance maneuvers. Section 3 provides on a brief description of the proposed dynamic model. Section 4 shows how the proposed control system was obtained from the previous dynamic model under nominal conditions. The dynamic behavior of the controlled system under non-nominal conditions is then presented in Section 5. Section 6 shows a comparison of the time responses of the controlled device under nominal and non-nominal conditions with the same controller, while Section 7 presents a detailed set of time responses of emersion/immersion maneuvers when large external disturbances are produced in the controlled system. Details of a new proposed trajectory reference are presented in Section 8. Finally, Section 9 illustrates experimental results obtained to validate both the proposed dynamic control and the performance of the proposed emersion/immersion strategy while Section 10 shows the conclusions of the work.

2. Manual and Automated Maneuvers for Gravity-Based First Generation TECs

In this section, we briefly describe the gravity-based first generation TECs as regards the manual and automated maneuvers required for their installation and maintenance. A complete and detailed description of the various stages of these maneuvers can be found in [34, 35]. Both papers present the GIT-ERM research group's recent developments concerning the calculations made to estimate to what extent the use of automated maneuvers would reduce the installation costs, in addition to the operation and maintenance costs. The conclusion was reached that these costs would be reduced by 10% and 15%, respectively.

There is little information on the installation and maintenance maneuvers of TECs owing to the fact that they are still being tested (i.e., they are in their pre-commercial phase), signifying that there is no real data related to the maneuvers that should be carried out. Nevertheless, it is possible to find general information regarding the installation of the devices being tested that enables us to form a fairly good idea of the maneuvers in question [21, 36, 37]. We, therefore, shall first study the way in which the maneuvers are carried out with these devices (manual control or in open loop), before going on to describe the GIT-ERM research group's engineering developments presented herein, which concern automated maneuvers (using the closed loop ballast control to reach the desired depth). Please note that certain parts are the same for both devices, i.e., those with open-loop maneuvers and those with closed-loop control maneuvers. The parts in question principally concern studying the area where the farm will be installed, in addition to the installation of the energy platform and bases. Readers requiring additional information on how the energy platform and bases are installed are referred to [21, 37, 38].

2.1. Manual Maneuvers

The concept of manual maneuvers is understood as the installation maneuvers of TECs using open loop, and that they are the maneuvers used for the installation of the first generation devices currently found in tests. The gondola must first be submerged and installed on the previously submerged base. Some designs, therefore, need special tools that "hug" the gondola (see Figure 1) and place it in the right place on the base [37, 38]. These tools are then removed once the gondola has been correctly positioned. Before carrying out the installation, which takes place on the deck of the special vessel (please note that the base on which the gondola will be placed must have been installed previously), the tool will grasp the gondola. Crane cables and the gondola recovery cables are connected to this tool, and these cables have

previously been recovered from the seabed or from the buoy where they had been arranged once the base installation was completed. This recovery cable, which is connected to the base, serves as a guide with which to properly locate the gondola. The gondola is, therefore, lowered with the crane, while controlling the descent speed, to the final position on the base, until the insertion is completed. Once the gondola is connected, the tool opens and it ascends to the special vessel. The guide wires are then disengaged and can, as before, be arranged on the seabed or in a buoy (both operations can be performed using a remote operated vehicle—ROV).

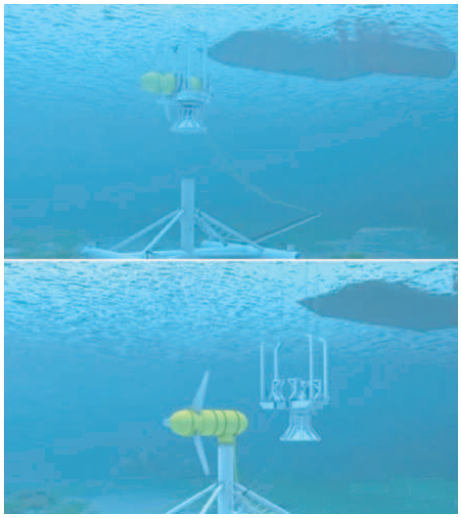

Figure 1: Gondola installation process using manual maneuvers.

A maintenance proposal for the device is described as follows [38]: (i) Blade cleaning. This is carried out in the same place where the TEC is located; (ii) Light preventive maintenance. All the equipment undergoes a service and general maintenance, comprising, among other things: changing the lubricating oil in the thrust bearing, changing the lubricating oil in the gearbox, refilling the compressed air bottles, a general review of all the components, cleaning the blades and checking to see whether the paint has any defects. The low level of complexity of this type of maintenance signifies that it can take place on board the special vessel, and (iii) High preventive maintenance, during which the gondola is disassembled and the following operations (among others) are carried out: the bearings of the thrust bearing are changed; the bearings of the gearbox are changed; the lubricating oil in the horn is changed, a general review of all the components is carried out, and the device is completely repainted. As will be clear from all of the above, the installation and recovery maneuvers of these devices require the use of special vessels with the following characteristics: (i) Dynamic positioning, in order to be able to work with redundancy and in extreme situations with a guarantee of safety and reliability. Vessels of this nature are extremely costly in both the technological and the economic sense [39, 40, 41, 42]; (ii) A heavy lifting crane, whose capacity should, according to [38], be approximately 250 tons of elevation, and (iii) A large deck area, which must be sufficiently large to enable the transportation of the devices, parts, gondolas, etc. that are going to be installed. As is evident from the above, the characteristics of the vessels required to install, maintain and recover these devices are not typical, signifying that it is not simple to find vessels of this nature for hire on the market. Moreover, special systems are required that increase the cost of constructing these vessels, which already exist and are being constructed for the oil and gas industry or in order to carry out the installation and maintenance of offshore wind farms. However, they are very expensive to hire and this cost varies according to the market, thus leading to great economic dependence on them [33, 34]. Furthermore, other vessels are required for the installation of the devices, in addition to the fact that there is also a need for other devices. As mentioned previously, ROVs are required in order to correctly locate the devices, while special vessels are needed to install the cables (cable ships) or carry out analyses

of the seabed (oceanographic vessels), etc., and their cost is also significant [36, 41, 42].

2.2. Automated Maneuvers

The above description of the maneuvers required to install the first-generation TECs currently being developed shows that these maneuvers are both complex and expensive. To this, the areas with greater currents and that are better suited to energy extraction from marine currents are areas with adverse weather and meteorological conditions [43], which increase the complexity of these maneuvers. This consequently led to the GIT-ERM research group's decision to employ a ballast control system for this purpose. This system will permit: (i) the gondola to be extracted from its normal depth of operation (on the seabed) up to the surface of the sea, and (ii) the subsequent return of the gondola to its base on the seabed. An illustration of a TEC that can carry out these automated maneuvers is shown in Figure 2, along with its main distribution equipment, located inside the gondola. Those readers who are interested in discovering the design modifications that permit the gondola to perform automated maneuvers or the experiments carried out with a laboratory prototype are referred to [15, 27, 44, 53]. Automated maneuvers of this nature will make it possible to reduce the resources required to both install and maintain the gondolas, which will in turn decrease the complexity and cost of these operations. This is of great interest as regards the future development of this renewable energy source.

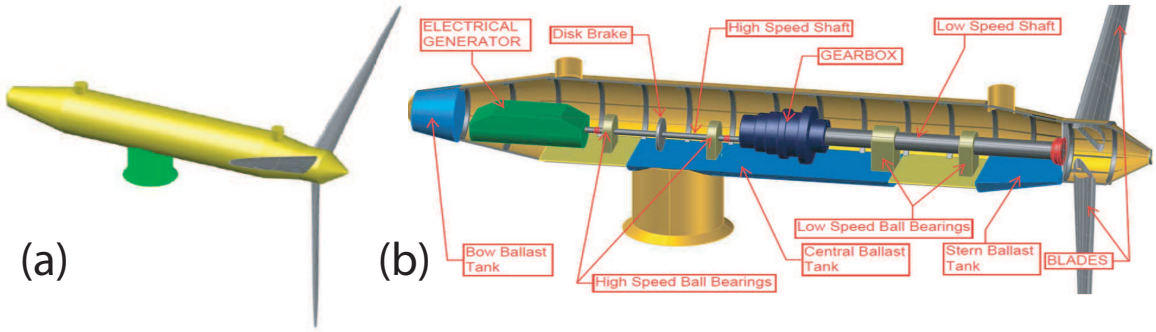

Figure 2: First generation TEC developed to carry out automated maneuvers: (**a**) Shape of the gondola and (**b**) Distribution equipment within the gondola.

Figure 3 shows how the gondola is installed using automated maneuvers. A tugboat takes the gondola to the place in which it will be installed. Once there, it is necessary to retrieve the umbilical cable, which is connected to the base. If the cable is on the seabed, an acoustic pulse is released that causes the cable to rise to the surface. The tugboat then approaches the cable and recovers it. This requires the services of a diver, who subsequently connects the cable to the gondola. It is now necessary to immerse the gondola in the water, which will done in two steps. First, the central ballast tank is filled with a pump for to increase the gondola's draught. When the top of the device is sumerged, the control system will be connected. This system is in carge of varying the ballast in the bow and stern tanks, it in order to make its weight greater than the thrust, which will allow it to descend. The smaller the difference between the thrust and the weight, the slower the descent will be. It is, therefore, necessary to lower the gondola vertically whilst simultaneously controlling the descent speed ballasting, which will be lesser or greater according to the speed required. The depth of the device can be controlled at all times by using acoustic/pressure depth sensors. The device is lowered to a depth near the top of the base. This operation additionally requires the use of a ROV for monitoring and control purposes.

It is supposed that the gondola is now at the depth required, but that it is not vertical to the base owing to the fact that the current prevents this. It is at this point that the umbilical cable is employed to help correctly locate the gondola on the base. This is done by placing a small winch, which works at a constant tension, in the union cylinder between the gondola and the base. The winch picks up the cable as the gondola is being submerged. Having located the gondola above the vertical part of the base, it is

again provided with sufficient ballast to allow it to descend onto the base, where it is then "fitted". The ballasting process makes it possible to control how fast or slow the gondola descends, since its speed can, at all times, be altered according to the amount of ballast introduced into the ballast tanks.

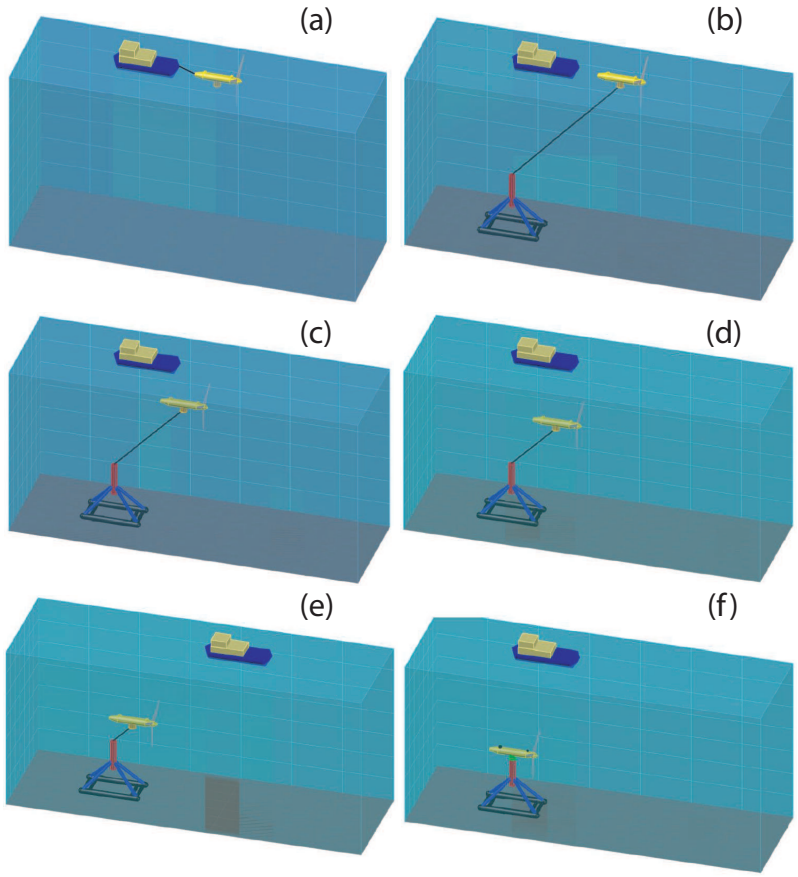

Figure 3: Gondola installation process using automated maneuvers: (**a**) Movement of the device with maneuver control in closed loop; (**b**) Connection between the cable wire and the gondola; (**c**) Immersion maneuver in closed loop; (**d**) Immersion maneuver in closed loop (cont.); (**e**) Immersion maneuver finished, and (**f**) Installation maneuver in closed loop finalized.

Finally, as occurs with the traditional manually maneuvered devices, there are various types of maintenance processes in the case of automated maneuvers: (i) Blade cleaning: the processes employed for the emersion and immersion of the gondola are faster than those required with the traditional maneuvers; (ii) Light preventive maintenance. The device with automated maneuvers has been designed by considering that the basic maintenance will be done "in situ", but the upload and reinstallation of the gondola will be faster and; (iii) High preventive maintenance: in this case, it is necessary to remove the gondola from the water and take it to dry land. Note that there are several advantages to the use of automated maneuvers: (a) The number of highly specialized vessels involved in the operation is reduced; (b) The time required to carry out maneuvering is also reduced, signifying that the weather window in which these installation and maintenance operations are performed can be also be reduced in those places in which these devices are available and where the weather is an important factor, and (c) The number of highly qualified personnel required to perform the maneuvers also decreases.

3. Brief Description of the Dynamic Model

According to the International Electrotechnical Commission and the Technical Committee "Marine Energy – Wave and tidal energy converters" [45] use a fixed reference frame $\{S_0\}$ to represent the position

and orientation of any kind of TEC (Tidal Energy Converter), which is referenced to a local reference frame $\{S\}$, as presented in Fig. 4.

The device coordinates are defined with regard to the fixed reference frame $\{S_0\}$ with the following orientation:

- The X-axis is perpendicular to the device plane, horizontal, and in the streamwise direction.
- The Z-axis is vertical and positive upwards.
- The Y-axis must form a Cartesian right-handed system with regard to the X and Z axes.

The origin of the fixed reference frame $\{S_0\}$ is located over the vertical part of the device and on the free surface of the sea.

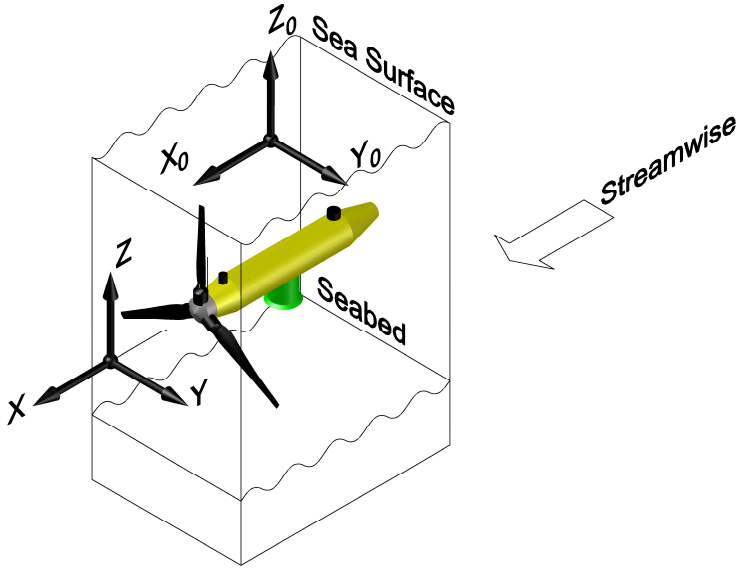

Figure 4: Fixed and local reference frame (taken from [15])

The simplest form of a TEC is obtained by joining the propeller (or the primary converter of the hydrokinetic energy into rotational energy) to an approximately cylindrical device. Fig. 5 shows a schematic representation of the submerged cylindrical body and the main magnitudes, the applied forces $f_1(t)$ and $f_2(t)$, the vertical forces produced by the actuators, which are represented on both sides of the cylindrical body, and the depth of the body, z.

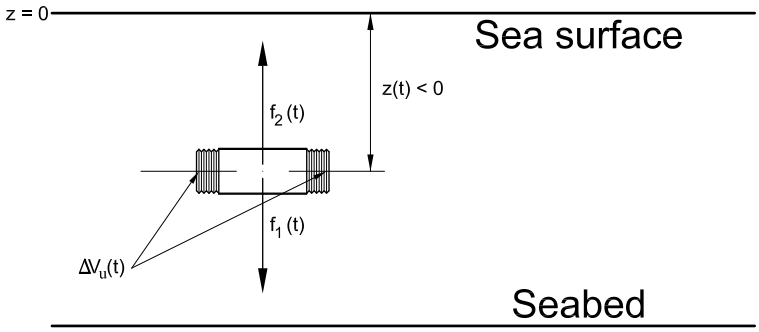

Figure 5: Main magnitudes of a submerged cylindrical body(taken from [15])

The equation for the dynamics of the submerged or semi-submerged body with one degree of freedom is given by:

$$\sum_i f_i(t) = (m + m_{Add}[z(t)]) \cdot \ddot{z}(t) + \nu \cdot \text{sign}\{\dot{z}(t)\} \cdot [\dot{z}(t)]^2 \tag{1}$$

where $f_1(t)$ and $f_2(t)$ are the only forces applied to the body in the absence of other external forces acting owing to the marine current, waves, effects of wind or others, all of which are considered to be external perturbations.

All forces and parameters are computed as follows:

$$\begin{aligned}
f_1(t) &= -m \cdot g && (2)\\
f_2(t) &= V(t) \cdot \rho_w(z, \theta, \text{Sal}) \cdot g && (3)\\
V(t) &= V_0 + \gamma \cdot z(t) + \Delta V_u(t) - V_{Buoy}[z(t)] + \Delta V(t) && (4)\\
\Delta V(t) &= \Delta F(t) \cdot \frac{1}{\rho_w(z, \theta, \text{Sal}) \cdot g} && (5)\\
m_{Add} &= m_{Add}[z(t)] && (6)\\
\rho_w &= \rho_w(z, \theta, \text{Sal}) && (7)\\
V_{Buoy} &= V_{Buoy}[z(t)] && (8)
\end{aligned}$$

The final result obtained from the terms modeled above is the dynamic model proposed in Eq. 1. If we substitute the forces provided in Eqs. 2 – 8, we obtain the following dynamic model of the submerged body which is represented in Fig. 6 as a block diagram.

$$\begin{aligned}
&[(V_0 + \gamma \cdot z(t) + \Delta V_u(t) - V_{Buoy} + \Delta V(t)) \cdot \rho_w - m] \cdot g = \\
= \;& (m + m_{Add}) \cdot \ddot{z}(t) + \nu \cdot \text{sign}(\dot{z}(t)) \cdot |\dot{z}(t)|^2
\end{aligned} \tag{9}$$

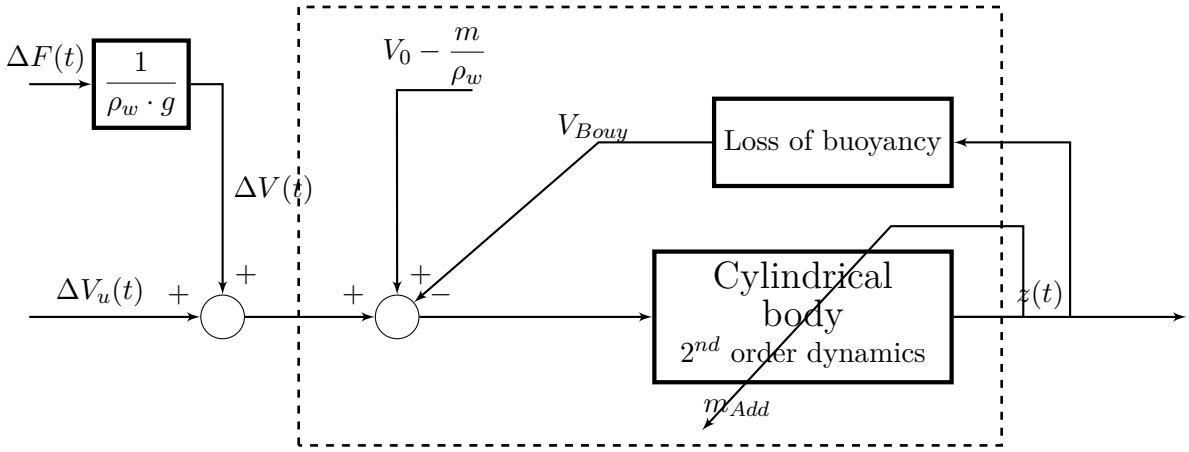

Figure 6: Dynamic model of the submerged body (adapted from [15])

The block diagram in Fig.6 shows the input variables, $\Delta V_u(t)$ and $\Delta F(t)$, which correspond with the non-modeled external disturbances and the output variable $z(t)$. In addition, the two main nonlinear terms proposed, added mass (m_{Add}) and the non-submerged volume of the cylinder, V_{Bouy}, are depth dependent. The V_{Bouy} is computed as an additive term, while the term m_{Add} is estimated as an element that modifies the inertia of the body. The main block of the dynamic model is, therefore, represented as

a block with variable dynamics that depends on the depth (Fig.6). A highly detailed stability analysis of this dynamic model was proposed in [15], which made is possible to prove that the device behaves in an unstable manner around the equilibrium point because of the compression term γ.

4. Closed loop Controller Desing

The proposed dynamic model can be employed to design different controllers for closed loop systems through the use of state-feedback techniques, because this makes it possible to assign poles to the feedback system in a simple algebraic form, in addition to guaranteeing the absence of open-loop zeros in the closed loop system that increase overshooting when step signals are used as a reference [46, 47, 48].

4.1. Linearization

The linearization of the dynamic model (Eq.9) around the equilibrium point is obtained from the following equation, which assumes that all the variables are incremental with respect to the point of linearization for nominal values (denoted with the sub-index $_0$) and under the conditions shown below:

- The added mass, m_{Add}, and the water density, ρ_w, are considered constants.
- The nominal volume, V_0, is equal to $\dfrac{m_0}{\rho_w}$.
- The body is fully submerged ($V_{Bouy} = 0$).
- In the absence of any kind of non-modeled external disturbances, $\Delta F(t) = 0$.

$$(\gamma_0 \cdot z(t) + \Delta V_u(t)) \cdot \rho_w \cdot g = (m_0 + m_{Add_0}) \cdot \ddot{z}(t) + 2 \cdot \nu_0 \cdot |\dot{z}_0| \cdot \dot{z}(t) \tag{10}$$

The control variable, $\Delta V_u(t)$ is solved as a function of the output variable, $z(t)$ and its derivatives, $\dot{z}(t)$ and $\ddot{z}(t)$.

$$\begin{aligned} \Delta V_u(t) &= \frac{m_0 + m_{Add_0}}{g \cdot \rho_w} \cdot \ddot{z}(t) + \frac{2 \cdot \nu_0 \cdot |\dot{z}_0|}{g \cdot \rho_w} \cdot \dot{z}(t) - \gamma_0 \cdot z(t) \\ &= \alpha_0 \cdot \ddot{z}(t) + \beta_0 \cdot \dot{z}(t) - \gamma_0 \cdot z(t) \end{aligned} \tag{11}$$

where the dynamic parameters, which have to be constants and nominal, considered for the linearized system are:

$$\begin{aligned} \alpha_0 &= \frac{m_0 + m_{Add_0}}{g \cdot \rho_w} > 0 \\ \beta_0 &= \frac{2 \cdot \nu_0 \cdot |\dot{z}_0|}{g \cdot \rho_w} \geq 0 \\ \gamma_0 &> 0 \end{aligned} \tag{12}$$

The associated state equations give rise to a linearized second order system with constant terms.

$$\begin{aligned} x_1(t) &= z(t) \\ \dot{x}_1(t) &= x_2(t) &&= \dot{z}(t) \\ \dot{x}_2(t) &= \ddot{z}(t) &&= \tfrac{\beta_0}{\alpha_0} x_2(t) + \tfrac{\gamma_0}{\alpha_0} x_1(t) + \tfrac{\Delta V_u(t)}{\alpha_0} \end{aligned} \tag{13}$$

The relationship in Eq. 13 allows the linearized dynamics to be expressed in a compact manner by using matrices in the controllable canonical form (from here on, the time-dependence is omitted).

$$\begin{aligned} \dot{\mathbf{x}} &= \mathbf{A}_0 \cdot \mathbf{x} + \mathbf{B}_0 \cdot \Delta V_u \\ z &= \mathbf{C}_0 \cdot \mathbf{x} \end{aligned} \tag{14}$$

which are:

$$\mathbf{A}_0 = \begin{pmatrix} 0 & 1 \\ \frac{\gamma_0}{\alpha_0} & -\frac{\beta_0}{\alpha_0} \end{pmatrix} \quad \mathbf{B}_0 = \begin{pmatrix} 0 \\ \frac{1}{\alpha_0} \end{pmatrix} \quad \mathbf{C}_0 = \begin{pmatrix} 1 & 0 \end{pmatrix} \tag{15}$$

The associated transfer function of the system can be obtained as follows. The compressibility coefficient, γ_0 is, therefore, a negative coefficient that causes the device to become unstable.

$$M_0(s) = \frac{Z(s)}{\Delta V_u(s)} = \mathbf{C}_0 \cdot (s\mathbf{I} - \mathbf{A}_0)^{-1} \cdot \mathbf{B}_0 = \frac{\frac{1}{\alpha_0}}{s^2 + s\frac{\beta_0}{\alpha_0} - \frac{\gamma_0}{\alpha_0}} \tag{16}$$

The associated controllability matrix (Eq. 17) shows that the system is fully controllable because of the determinant of the matrix results $\frac{-1}{\alpha_0^2} \neq 0$, and the rank of this matrix is, therefore, 2.

$$\mathbf{Q_0} = \begin{pmatrix} \mathbf{B}_0 & \mathbf{A}_0 \cdot \mathbf{B}_0 \end{pmatrix} = \begin{pmatrix} 0 & \frac{1}{\alpha_0} \\ \frac{1}{\alpha_0} & -\frac{\beta_0}{\alpha_0^2} \end{pmatrix} \tag{17}$$

The possibility of designing a controller that allows the poles of the feedback system to be placed in the desired positions of the complex plane and the use of state feedback techniques is, therefore, justified [49, 50, 51]. Two kinds of controllers are presented as follows:

4.2. PD controller type

The state feedback proposed at this point is equivalent to that provided by a Proportional-Derivative controller type (see Fig.7), denominated as PD, when the derivative feedback term is taken from the output (rather than from the error).

$$\Delta V_u = z_{ref} + \mathbf{K}_{F0} \cdot \mathbf{x} \tag{18}$$

This feedback signal (Eq.18) modifies the dynamics of the system (Eq. 14), obtaining the following equation of the closed loop system, where $\mathbf{K}_{F0} = \begin{pmatrix} k_{f1} & k_{f2} \end{pmatrix}$ denotes the state gain matrix.

$$\begin{aligned} \dot{\mathbf{x}} &= \overbrace{(\mathbf{A}_0 + \mathbf{B}_0 \cdot \mathbf{K}_{F0})}^{\mathbf{A}_{C0}} \cdot \mathbf{x} + \mathbf{B}_0 \cdot z_{ref} \\ z &= \mathbf{C}_0 \cdot \mathbf{x} \end{aligned} \tag{19}$$

With this proposed controller, the signal $z_{ref}(t)$ is used as a reference, and the complete dynamics of the system can be modified by the gain matrix, $\mathbf{K}_{F0}$. The design poles selected for the closed loop system correspond to a critically damping second order system with a time constant "a". The characteristic polynomial, $\phi_{PD}(s)$, as a function of the designed parameter, "a", is equivalent to the denominator of the transfer function with the coefficient being the higher order of unit value.

$$\phi_{PD}(s) = s^2 + 2as + a^2 \tag{20}$$

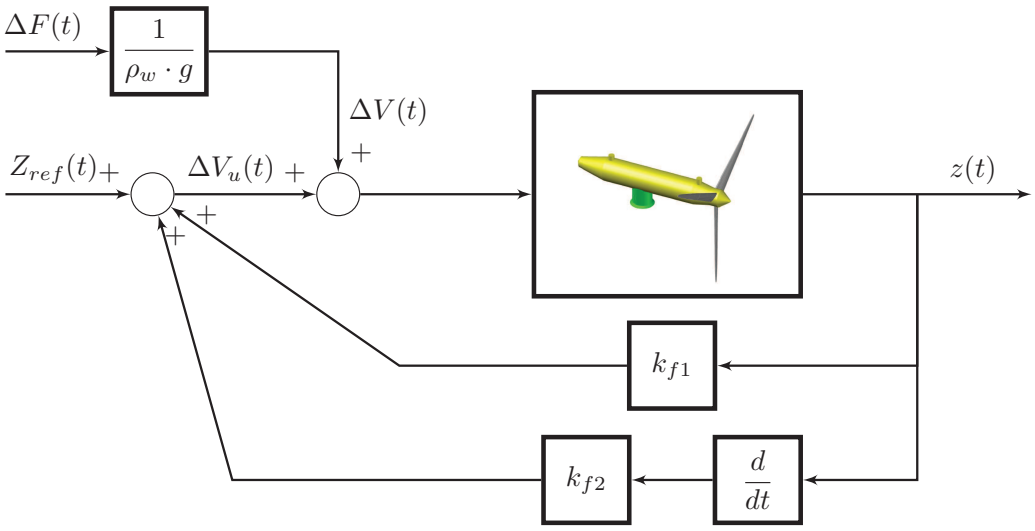

Figure 7: The state feedback with PD controller type.

By decomposing the gain matrix, $\mathbf{K}_{F0}$ and by placing the poles in the system in the controllable canonical form, we obtain:

$$\mathbf{A}_{C0} = \begin{pmatrix} 0 & 1 \\ -a^2 & -2a \end{pmatrix} = \begin{pmatrix} 0 \\ \frac{1}{\alpha_0} \end{pmatrix} \cdot \begin{pmatrix} k_{f1} & k_{f2} \end{pmatrix} + \begin{pmatrix} 0 & 1 \\ \frac{\gamma_0}{\alpha_0} & -\frac{\beta_0}{\alpha_0} \end{pmatrix} \tag{21}$$

The gains of the desired feedback-state matrix for the nominal values of the parameters are simply determined from this equation:

$$\mathbf{K}_{F0} = \begin{pmatrix} k_{f1} & k_{f2} \end{pmatrix} = \begin{pmatrix} -a^2\alpha_0 - \gamma_0 & -2a\alpha_0 + \beta_0 \end{pmatrix} \tag{22}$$

Finally, by replacing Eq. 22 in Eq. 19 the transfer function between the reference depth, $Z_{ref}(s)$, and the real depth, $Z(s)$, of the device for the proposed controller is obtained (signals in the Laplace Domain):

$$M_{PD_0}(s) = \frac{Z(s)}{Z_{ref}(s)} = \frac{\frac{1}{\alpha_0}}{s^2 + 2as + a^2} \tag{23}$$

For this transfer function to be of unit gain, it is necessary to add a gain that modifies the numerator. The relationship between the reference and the output variable, therefore, results in a null steady state error in the absence of external perturbations. This gain is placed as a filtering term whose value is $k_0 = \alpha_0 a^2$. In order to avoid this filtering gain with a desired closed loop dynamics, a PID controller is explored [52].

4.3. I-PD Controller type

A slightly modified Proportional-Integral Derivative or PID controller (denominated as called I-PD and shown in Fig.8) is proposed, because the derivative part intervenes only as regards the output signal, thus avoiding the presence of zeros of the controller that would cause unplanned overshoots in the case of employing step functions of rapid variations as inputs. The proportional term is also in the output. A virtual variable is created, $x_\varepsilon(t)$, and this is obtained by integrating the error between the reference and the output.

$$x_\epsilon(t) = \int_0^t \dot{x}_\epsilon(\tau) d\tau = \int_0^t \left[z_{ref}(\tau) - z(\tau) \right] d\tau \tag{24}$$

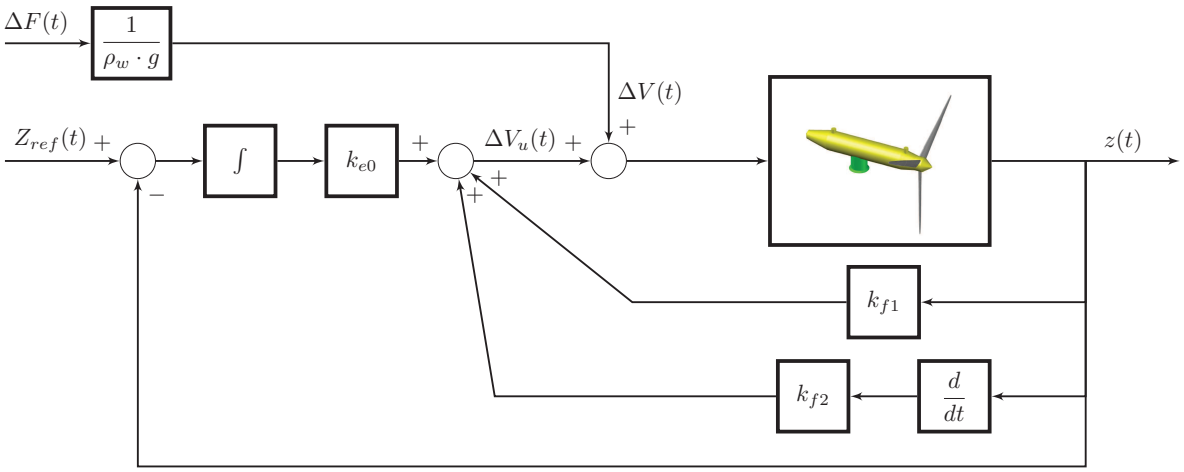

Figure 8: The state feedback with I-PD controller type.

The new feedback term of the system increases the order of the system owing to the addition of the variable $x_\epsilon(t)$, thus allowing the following matrix equation to be obtained:

$$\begin{pmatrix} \dot{x}_\epsilon \\ \dot{\mathbf{x}} \end{pmatrix} = \begin{pmatrix} 0 & -\mathbf{C}_0 \\ \mathbf{0} & \mathbf{A}_0 \end{pmatrix} \cdot \begin{pmatrix} x_\epsilon \\ \mathbf{x} \end{pmatrix} + \begin{pmatrix} 0 \\ \mathbf{B}_0 \end{pmatrix} \cdot \Delta V_u + \begin{pmatrix} 1 \\ \mathbf{0} \end{pmatrix} \cdot z_{ref} \tag{25}$$

The zero matrix of dimension 2×1 is denoted as $\mathbf{0}$ in order to differentiate it from a null scalar value, which is simply denoted as 0. The proposed state feedback is now of the form shown below:

$$\Delta V_u = k_{\epsilon 0} \cdot x_\epsilon + \mathbf{K}_{FE0} \cdot \mathbf{x} \tag{26}$$

The state vector is now denoted as $\widehat{\mathbf{x}}(t) = \begin{pmatrix} x_\epsilon(t) & \mathbf{x}(t) \end{pmatrix}^T$. This vector, together with the previous state feedback (Eq. 26), modifies the dynamics of the system (Eq. 25) as shown in the following equation, which is equivalent to an I-PD controller described previously.

$$\begin{aligned} \dot{\widehat{\mathbf{x}}} &= \overbrace{\left[\begin{pmatrix} 0 & -\mathbf{C}_0 \\ \mathbf{0} & \mathbf{A}_0 \end{pmatrix} + \begin{pmatrix} 0 \\ \mathbf{B}_0 \end{pmatrix} \cdot \begin{pmatrix} k_{\epsilon 0} & \mathbf{K}_{FE0} \end{pmatrix} \right]}^{\widehat{\mathbf{A}}_{C0}} \cdot \widehat{\mathbf{x}} + \begin{pmatrix} 1 \\ \mathbf{0} \end{pmatrix} \cdot z_{ref} \\ z &= \begin{pmatrix} 0 & \mathbf{C}_0 \end{pmatrix} \cdot \widehat{\mathbf{x}} \end{aligned} \tag{27}$$

The location of the poles from the feedback system can be modified through the use of a characteristic polynomial, $\widehat{\phi}_{I-PD}(s)$, in this case, of third order. All the roots of the desired characteristic polynomial are real and are defined by employing two design parameters, "a" and "b", as follows:

$$\widehat{\phi}_{I-PD}(s) = (s+a) \cdot \left(s^2 + 2bs + b^2 \right) \tag{28}$$

It is easy to verify that the time response of the controlled system for the previous characteristic polynomial, when $b = 2a$ or using the characteristic polynomial from Eq.20, are similar. Fig.9 shows the time response under a step signal input for both systems with the unit gain.

Note that both time responses are similar, thus making the slope of the time response in $t = 0$, the rise time, t_r, settling time t_s, and a null overshoot, M_p, identical in both cases. The third order desired characteristic polynomial as a unique parameter "a" function is:

$$\widehat{\phi}_{I-PD_0}(s) = s^3 + 5as^2 + 8a^2 s + 4a^3 \tag{29}$$

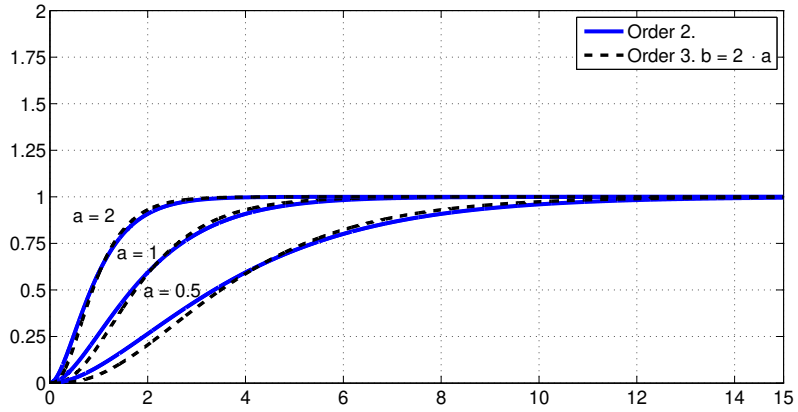

Figure 9: Time response for a 2nd and 3rd order system when $b = 2a$.

The desired location of the closed loop poles of the system makes it possible to obtain the new gain matrix $\widehat{\mathbf{K}}_{F0} = \begin{pmatrix} k_{\epsilon 0} & K_{FEO} \end{pmatrix} = \begin{pmatrix} k_{\epsilon 0} & k_{f1} & k_{f2} \end{pmatrix}$ from the following equality:

$$\begin{aligned} \widehat{\mathbf{A}}_{C0} &= \begin{pmatrix} 0 & -1 & 0 \\ 0 & 0 & 1 \\ 4a^3 & -8a^2 & -5a \end{pmatrix} \\ &= \begin{pmatrix} 0 \\ 0 \\ \dfrac{1}{\alpha_0} \end{pmatrix} \cdot \begin{pmatrix} k_{\epsilon 0} & k_{f1} & k_{f2} \end{pmatrix} + \begin{pmatrix} 0 & -1 & 0 \\ 0 & 0 & 1 \\ 0 & \dfrac{\gamma_0}{\alpha_0} & -\dfrac{\beta_0}{\alpha_0} \end{pmatrix} \end{aligned} \tag{30}$$

This equality allows us to obtain the gain matrix in a simple and direct manner:

$$\begin{pmatrix} k_{\epsilon 0} & k_{f1} & k_{f2} \end{pmatrix} = \begin{pmatrix} 4a^3\alpha_0 & -8a^2\alpha_0 - \gamma_0 & -5a\alpha_0 + \beta_0 \end{pmatrix} \tag{31}$$

The closed loop system dynamics with the previous matrix becomes the following third order transfer function between $Z_{ref}(s)$ and $Z(s)$.

$$M_{I-PD_0}(s) = \frac{Z(s)}{Z_{ref}(s)} = \frac{4a^3}{s^3 + 5as^2 + 8a^2s + 4a^3} \tag{32}$$

This transfer function makes it possible to verify that the poles are in the desired location and that the numerator coincides with the independent term of the denominator, which guarantees a null steady state under step type input signals.

5. Dynamic Behavior under Non-Nominal Conditions (NNC)

Under the realistic hypothesis of the incorrect assignment of the parameters of the system to real values, in this section the effect of that errors or uncertainties of the dynamic model have on the system in closed loop for the designed controller is studied. These errors or uncertainties are, in this case, to be only parametric uncertainties. These conditions are denominated as non-nominal (NNC).

5.1. Controller type PD under NNC

The new matrix of the controller system with non-nominal parameters and the same nominal gain matrix obtained for the PD controller (Eq.22), in which the sub-index $_0$ is omitted because the constants are non-nominal, becomes:

$$\begin{aligned} \dot{\mathbf{x}} &= \overbrace{(\mathbf{A}+\mathbf{B}\cdot\mathbf{K}_{F0})}^{\mathbf{A}_C}\cdot\mathbf{x} + \mathbf{B}\cdot z_{ref} \\ z &= \mathbf{C}\cdot\mathbf{x} \end{aligned} \tag{33}$$

where the matrix $\mathbf{A}_C$ developed is:

$$\begin{aligned} \mathbf{A}_C &= \begin{pmatrix} 0 & 1 \\ \frac{\gamma}{\alpha} & -\frac{\beta}{\alpha} \end{pmatrix} + \begin{pmatrix} 0 \\ \frac{1}{\alpha} \end{pmatrix} \cdot \begin{pmatrix} k_{f1} & k_{f2} \end{pmatrix} = \\ &= \begin{pmatrix} 0 & 1 \\ -\frac{\alpha_0 a^2+\gamma_0-\gamma}{\alpha} & -\frac{2a\alpha_0+\beta-\beta_0}{\alpha} \end{pmatrix} \end{aligned} \tag{34}$$

where α, β and γ are the same as in Eq. 12, but this parameter now denotes the non-nominal values. On this occasion, the characteristic polynomial and the transfer function are:

$$\phi_{PD_{NN}}(s) = s^2 + s\frac{2a\alpha_0+\beta-\beta_0}{\alpha} + \frac{\alpha_0 a^2+\gamma_0-\gamma}{\alpha} \tag{35}$$

$$M_{PD}(s) = \frac{Z(s)}{Z_{ref}(s)} = \frac{\frac{\alpha_0 a^2}{\alpha}}{s^2 + s\frac{2a\alpha_0+\beta-\beta_0}{\alpha} + \frac{\alpha_0 a^2+\gamma_0-\gamma}{\alpha}} \tag{36}$$

which correspond to the respective nominal value transfer function (Eq.23) only when $\alpha = \alpha_0$, $\beta = \beta_0$ and $\gamma = \gamma_0$. For small variations in the parameters that define the open-loop system and for high values of parameter a (faster dynamics and poles farther from the imaginary axis than the dynamics of the system without feedback), it is verified that the transient state of the feedback system is not substantially modified. However, the time response in the steady state under non-nominal conditions can be obtained by simply applying the final value theorem with $Z_{ref}(s)$ defined as a step input.

$$\lim_{t\to\infty}\frac{z(t)}{z_{ref}(t)} = \lim_{s\to 0} s\cdot\frac{Z(s)}{Z_{ref}(s)} = \lim_{s\to 0}\frac{\frac{\alpha_0 a^2}{\alpha}}{s^2 + s\frac{2a\alpha_0+\beta-\beta_0}{\alpha} + \frac{\alpha_0 a^2+\gamma_0-\gamma}{\alpha}} \neq 1 \tag{37}$$

This signifies that, in the absence any kind of external disturbances, a simple error in the modeling of the compressibility coefficient, γ, does not allow obtain time responses with null errors to be obtained.

5.2. Controller type I-PD under NNC

The behavior of this second controller will be verified in a similar way as in the previous case. The new feedback system of non-nominal parameters with the nominal gain matrix from Eq. 31 results in:

$$\begin{aligned} \dot{\hat{\mathbf{x}}} &= \overbrace{\left[\begin{pmatrix} 0 & -\mathbf{C} \\ \mathbf{0} & \mathbf{A} \end{pmatrix} + \begin{pmatrix} 0 \\ \mathbf{B} \end{pmatrix}\cdot\begin{pmatrix} k_{\epsilon 0} & \mathbf{K}_{FE0} \end{pmatrix}\right]}^{\widehat{\mathbf{A}}_C}\cdot\hat{\mathbf{x}} + \begin{pmatrix} 1 \\ \mathbf{0} \end{pmatrix}\cdot z_{ref} \\ z &= \begin{pmatrix} 0 & \mathbf{C} \end{pmatrix}\cdot\hat{\mathbf{x}} \end{aligned} \tag{38}$$

The $\widehat{\mathbf{A}}_C$ developed is:

$$\begin{aligned}\widehat{\mathbf{A}}_C &= \begin{pmatrix} 0 & -1 & 0 \\ 0 & 0 & 1 \\ 0 & \frac{\gamma}{\alpha} & -\frac{\beta}{\alpha} \end{pmatrix} + \begin{pmatrix} 0 \\ 0 \\ \frac{1}{\alpha} \end{pmatrix} \cdot \begin{pmatrix} k_{\epsilon 0} & k_{f1} & k_{f2} \end{pmatrix} = \\ &= \begin{pmatrix} 0 & -1 & 0 \\ 0 & 0 & 1 \\ 4a^3\frac{\alpha_0}{\alpha} & -\frac{8a\alpha_0+\gamma_0-\gamma}{\alpha} & -\frac{5a\alpha_0+\beta-\beta_0}{\alpha} \end{pmatrix}\end{aligned} \tag{39}$$

For this controller, both the characteristic polynomial and the transfer function are, respectively:

$$\widehat{\phi}_{I-PD_{NN}}(s) = \left[s^3 + s^2\left(\frac{5a\alpha_0+\beta-\beta_0}{\alpha}\right) + s\left(\frac{8a\alpha_0+\gamma_0-\gamma}{\alpha}\right) + 4a^3\frac{\alpha_0}{\alpha}\right] \tag{40}$$

$$M_{I-PD}(s) = \frac{Z(s)}{Z_{ref}(s)} = \frac{4a^3\frac{\alpha_0}{\alpha}}{s^3 + s^2\left(\frac{5a\alpha_0+\beta-\beta_0}{\alpha}\right) + s\left(\frac{8a\alpha_0+\gamma_0-\gamma}{\alpha}\right) + 4a^3\frac{\alpha_0}{\alpha}} \tag{41}$$

which correspond to the respective nominal value transfer function (Eq.32) when $\alpha = \alpha_0$, $\beta = \beta_0$ and $\gamma = \gamma_0$.

In steady state, the time response is null error under non-nominal conditions. In other words, the time response tracks the reference for the I-PD controller, which can be checked by applying the final value theorem when $Z_{ref}(s)$ is a step input.

$$\lim_{t\to\infty}\frac{z(t)}{z_{ref}(t)} = \lim_{s\to 0}\frac{Z(s)}{Z_{ref}(s)} = \lim_{s\to 0}\frac{4a^3\frac{\alpha_0}{\alpha}}{s^3 + s^2\left(\frac{5a\alpha_0+\beta-\beta_0}{\alpha}\right) + s\left(\frac{8a\alpha_0+\gamma_0-\gamma}{\alpha}\right) + 4a^3\frac{\alpha_0}{\alpha}} = 1 \tag{42}$$

Regardless of the variations associated with the parametric uncertainties of the open-loop system, this controller guarantees that time responses with null errors in steady state will be obtained independently of the error committed in the dynamic modeling of the system or parameter uncertainties.

The behavior in the transient state is now verified in two ways for the I-PD nominal controller. The parameter α is related to the mass together with its added mass, while the β parameter is obtained from the linearization of the viscous friction of the quadratic character for a certain speed of operation, which is also variable. The following study is carried out in the next range of variation of the parameters of the α and β system, which is much wider than the maximum variations expected in reality.

$$\begin{aligned}\frac{\alpha_0}{2} &\leq \alpha \leq 2\alpha_0 \\ \frac{\beta_0}{10} &\leq \alpha \leq 10\beta_0\end{aligned} \tag{43}$$

The variations in the compressibility coefficient with respect to its nominal value are not considered here because its value is very small. The modification of the location of the poles of the feedback system in the complex plane when compared to its nominal location is initially analyzed by studying the variations in its α and β parameters (Eq. 43). The location of the three poles of the closed loop system is provided by a characteristic polynomial (Eq. 29). These poles are: $p_{10} = -a$ and $p_{20} = p_{30} = -2a$.

Fig. 10 shows three graphs, each of which corresponds to the location of the poles for different values of the design parameter a, which are 0.01, 0.02 and 0.04 rad/s, respectively, for the α range.

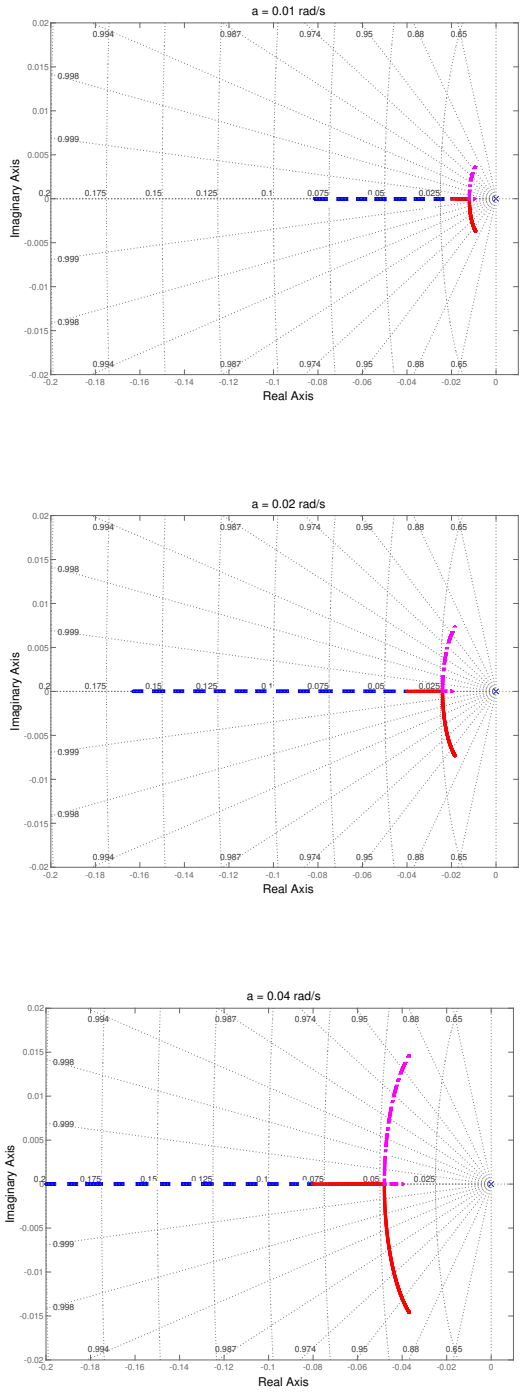

Figure 10: Location of closed loop poles with I-PD nominal controller and $\frac{\alpha_0}{2} \leq \alpha \leq 2\alpha_0$.

Fig.11 shows a group of graphs similar to those depicted previously for the same values of the α parameter, but in this case, the graphs correspond to the variations in the β parameter.

The small variation in the dominant poles can be noted in both groups of graphs. In this case, the poles are closer to the origin in the complete range of the α and β parameters.

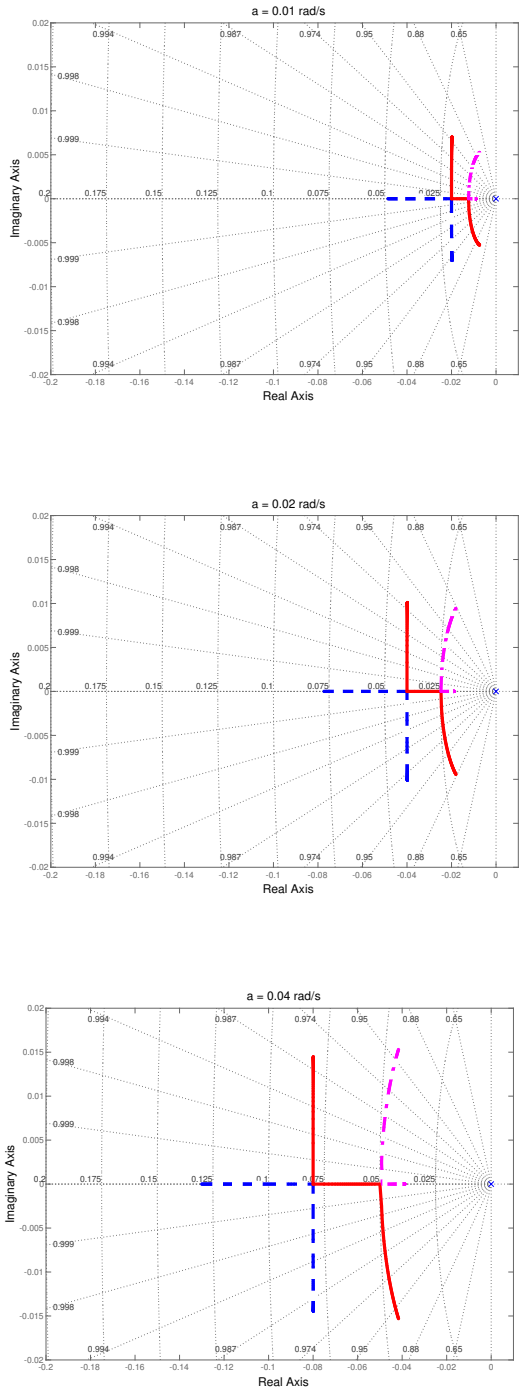

Figure 11: Location of closed loop poles with I-PD nominal controller and $\frac{\beta_0}{2} \leq \beta \leq 2\beta_0$.

Finally, we shall now analyze the transient step response properties of the output signals, also supposing that a step input signal is applied, when the characteristic polynomial is non-nominal and the dynamic parameters of the device in open loop, thus providing great differences with respect to the nominal values, for the same range of the α and β parameters. For this, the following transient step response properties, have been selected for this purpose:

- t_r: Rise time, measured as the time the system takes to modify its depth from 10-90% of its reference.

- t_s: Settling time, measured as the time taken by the step response to achieve an error of less than 2%.
- M_p: Overshoot or percentage of the maximum value of the time response supposing that a step function is applied when compared to the final value in the steady state.

Figs. 12, 13 and 14 show the variation in the transient step response properties t_r, t_s and M_p, respectively, supposing that input step signal is applied and for the previously given range for α and β (Eq. 43), when parameter $a = 0.01 rad/s$. The nominal values are also represented, and are: $t_r = 292s$, $t_s(2\%) = 528s$ and $M_p = 0\%$.

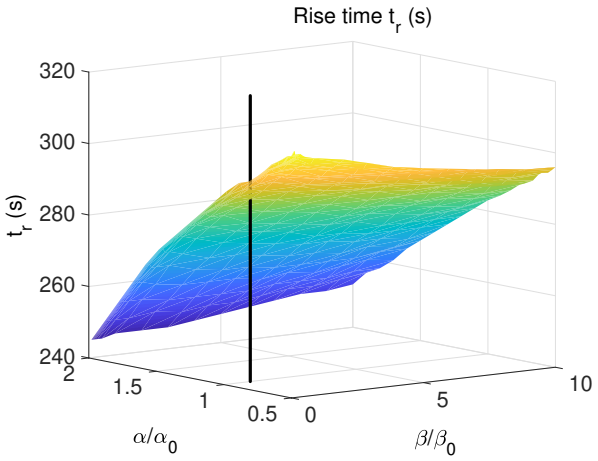

Figure 12: Rise time for $a = 0.01 rad/s$ and variations of α and β

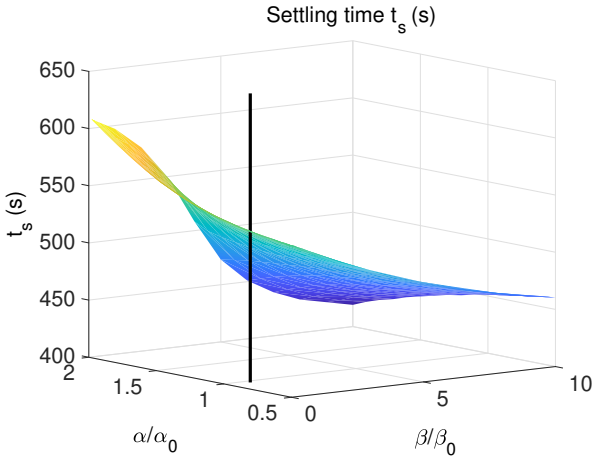

Figure 13: Settling time for $a = 0.01 rad/s$ and variations of α and β

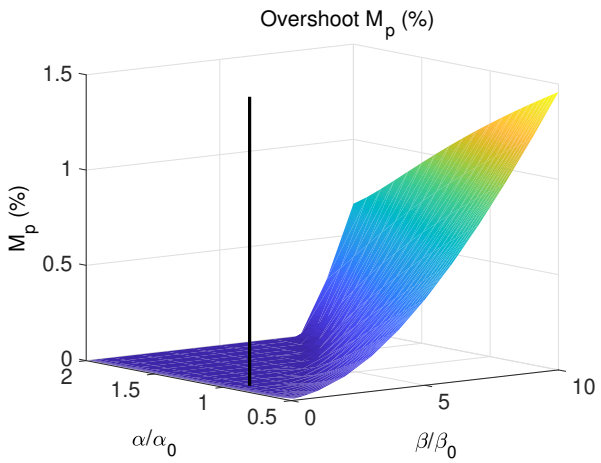

Figure 14: Overshoot (%) for $a = 0.01 rad/s$ and variations of α and β

Figs. 15, 16, 17 present the variations in t_r, t_s and M_p supposing that step input signal is applied for the same range of α and β provided in Eq. 43, but the value of the design parameter "a" is now $0.02 rad/s$. The nominal values have also been represented: $t_r = 146s$, $t_s(2\%) = 265s$ and $M_p = 0\%$. Figs. 18, 19 and 20, meanwhile, reveal the same as the previous ones when $a = 0.04 rad/s$, and the expected nominal values are: $t_r = 73s$, $t_s(2\%) = 132s$ and $M_p = 0\%$.

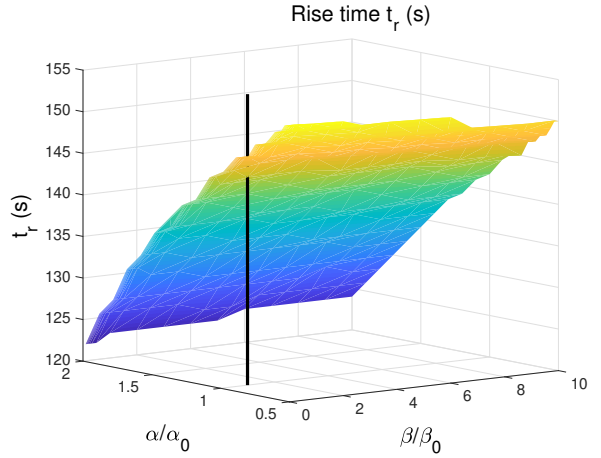

Figure 15: Rise time for $a = 0.02 rad/s$ and variations of α and β

For the range studied, the maximum value of overshoots, M_p, appears when $\alpha = \alpha_0/2$ and $\beta = 10\beta_0$ (the greatest is 1.5% for $a = 0.01 rad/s$), as can be concluded from Figs. 14, 17 and 20. The variations in the rise time, t_r, and the settling time, t_s, are small for any value of the parameter β, as can be observed in Figs. 12, 13, 15, 16, 18 and 19. In consequence, the controller obtained from Eq. 31 is used under nominal conditions, and please recall that, as the parameter α is related to the added mass, it can be clearly seen (flatness zone in Figs. 14, 17 and 20) that the use of the maximum expected added mass, rather than the nominal one, is a better criterion for the controller, because of the absence of overshooting.

The variation in the transient step response properties is smaller when the nominal design poles move away from the origin. It is for this reason that the value of design parameter, "a", must be chosen according to the smallest possible variation of the transient response for the maximum possible parametric variations, and the maximum capacity of the actuators. It is for this reason that $a = 0.02 rad/s$ has been chosen for the following sections.

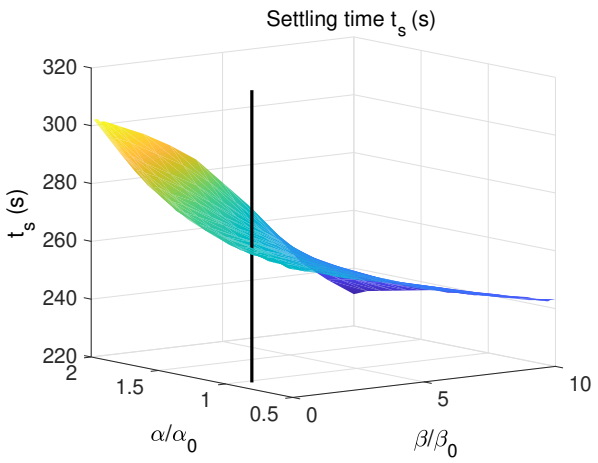

Figure 16: Settling time for $a = 0.02 rad/s$ and variations of α and β

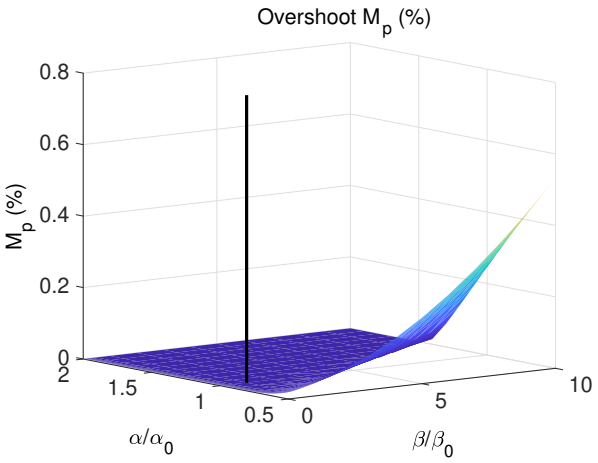

Figure 17: Overshoot (%) for $a = 0.02 rad/s$ and variations of α and β

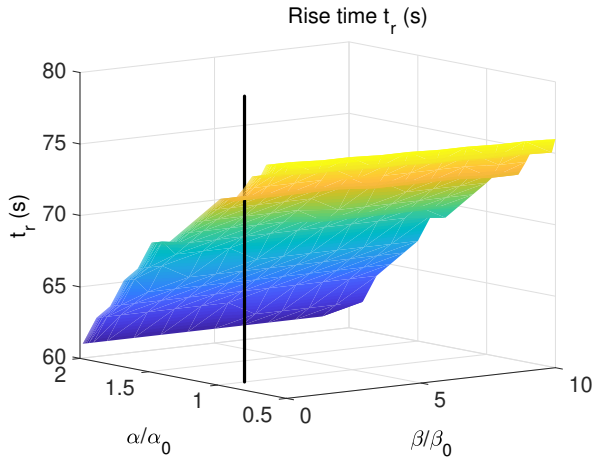

Figure 18: Rise time for $a = 0.04 rad/s$ and variations of α and β

6. Time Responses under NNC

In this section, different time responses of the controlled system under non-nominal conditions (NNC) can be seen when the device is near to the free surface for the two previously designed controllers, when

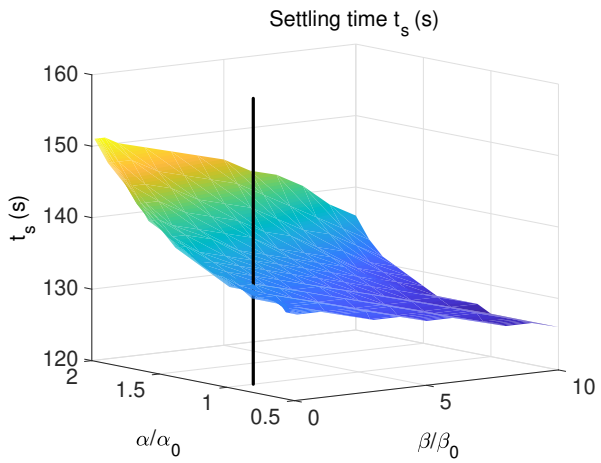

Figure 19: Settling time for $a = 0.04 rad/s$ and variations of α and β

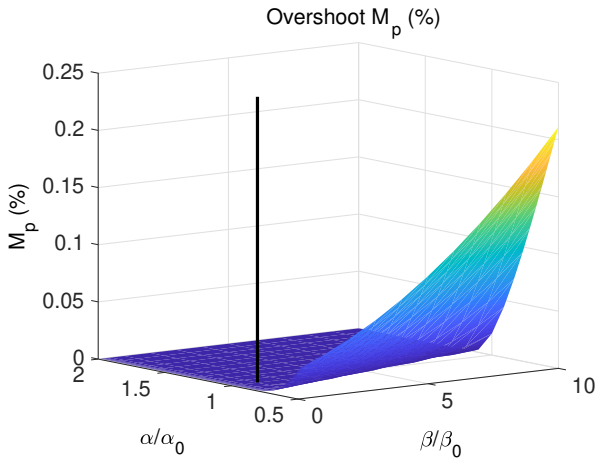

Figure 20: Overshoot (%) for $a = 0.04 rad/s$ and variations of α and β

the next input signal used as a reference is:

$$z_{ref}(t) = \begin{cases} -5 \quad m \quad \text{for} \quad 0 \quad s \leq t < 100 \quad s \\ -1.25 \quad m \quad \text{for} \quad 100 \quad s \leq t < 1400 \quad s \\ -3.25 \quad m \quad \text{for} \quad 1400 \quad s \leq t \leq 3000 \quad s \end{cases} \tag{44}$$

Two types of simulations are analyzed for each controller. The first corresponds with the different time responses of the controller when the friction coefficient variation, supposing that the value is both double the nominal value and half the nominal value (i.e. $\nu = \nu_0 \cdot 2$ and $\nu = \nu_0/2$). The second corresponds with the different time responses of the controller system supposing that the value of the added mass is both double the added mass and half the added mass of the device in a movement for any depth (i.e. $m_{Add} = m_{Add} \cdot 2$ and $m_{Add} = m_{Add}/2$). The zoom of the transient section when the device is close to the surface is also included, but the zoom of the transient section for the submerged device is omitted.

6.1. PD controller type under NNC

The small variation in the time responses for the variations in viscous friction is shown in Fig. 21, while Fig. 22 shows that the time responses of the feedback system undergo a clear deterioration when the device is close to the free surface and the added mass corresponds to a double nominal value.

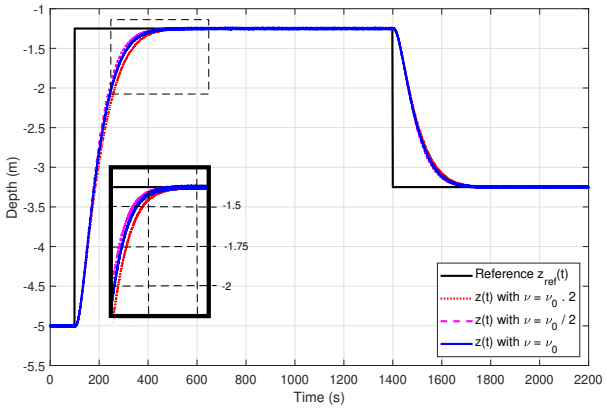

Figure 21: Time response with the PD controller with ν variations

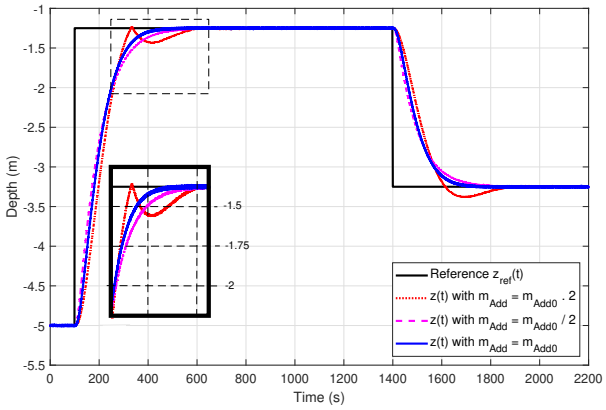

Figure 22: Time response with the PD controller with m_{Add} variations

6.2. I-PD controller type under NNC

The variation in the time responses, supposing that different values of vicious friction are small, as will be noted in Fig. 23. A minor influence of the variation in the added mass term can be noted in the time responses of the simulations shown in Fig. 24.

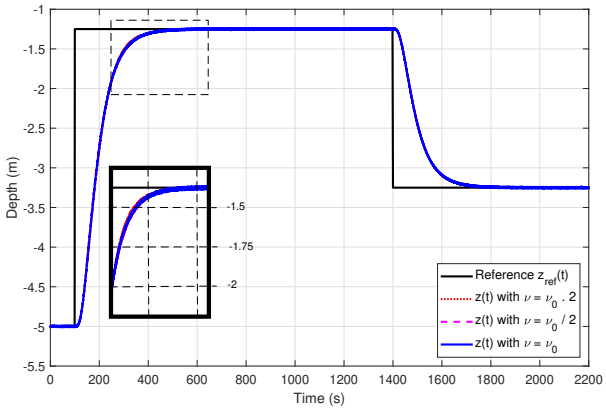

Figure 23: Time response for I-PD controller with ν variations

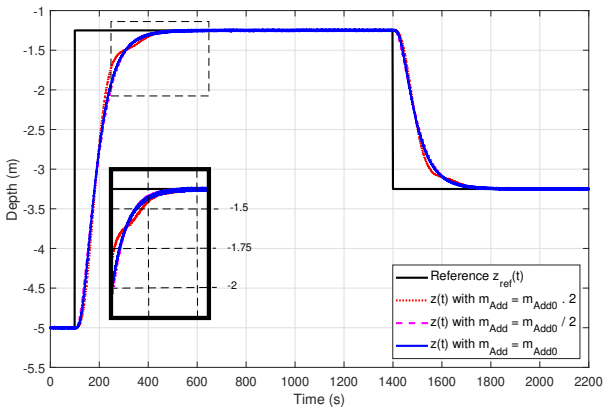

Figure 24: Time response for I-PD controller with m_{Add} variations

7. Presence of Additive Disturbances (AD)

The aim of this section is to analyze the effects of additive disturbances (AD), which has until now been considered zero, on the time response of the feedback close loop system with the previously designed controllers. The possibility of the incorrect assignment of the system parameters to their real values is also taken into account.

Any additive term can be considered as a volume disturbance, $\Delta V_D(t)$ (Eq.45), with respect to the lineal system and even to the non-nominal conditions. The different disturbances have been contemplated:

- ΔV_{Bouy}, which can easily be computed in real-time by means of geometrical considerations [15, 53].
- $V_0 - \dfrac{m}{\rho_w}$, which is $\neq 0$ when $m \neq m_0$ owing to the effects of corrosion ($V_0 - \dfrac{m}{\rho_w} > 0$) or biofouling ($V_0 - \dfrac{m}{\rho_w} < 0$).
- The remaining non-modeled forces, $\Delta F(t)$, are computed as volume disturbances by simply scaling $\dfrac{\Delta F(t)}{\rho_w \cdot g}$, which have been represented in Fig. 6 as volume external disturbances, $\Delta V(t)$, outside the main block (dashed line).

$$\Delta V_D(t) = -V_{Bouy} + \left(V_0 - \frac{m}{\rho_w}\right) + \Delta V(t) \tag{45}$$

If Eq. 9 is linearized around the equilibrium point for nominal values, it is possible to obtain the relationship between the two simultaneous input signals, $\Delta V_u(t)$ and $\Delta V_D(t)$, and the output signal, $z(t)$. The following equation is obtained, and again represents the system in open-loop.

$$(\gamma_0 \cdot z(t) + \Delta V_u(t) + \Delta V_D(t)) \cdot \rho_w \cdot g = (m_0 + m_{Add_0}) \cdot \ddot{z}(t) + 2 \cdot \nu_0 \cdot |\dot{z}_0| \cdot \dot{z}(t) \tag{46}$$

Under the hypothesis that the additive disturbance $\Delta V_D(t)$ is Laplace transformable as $\mathcal{L}[\Delta V_D(t)] = \Delta V_D(s)$, the transfer function for open-loop would remain as follows:

$$Z(s) = \frac{\frac{\Delta V_u(s)}{\alpha_0}}{s^2 + s\dfrac{\beta_0}{\alpha_0} - \dfrac{\gamma_0}{\alpha_0}} + \frac{\frac{\Delta V_D(s)}{\alpha_0}}{s^2 + s\dfrac{\beta_0}{\alpha_0} - \dfrac{\gamma_0}{\alpha_0}} \tag{47}$$

In this section, it is also assumed that $\lim_{s\to 0} Z_{ref}(s) = Z_{ref}$ and $\lim_{s\to 0} \Delta V_D(s) = \Delta V_D$.

7.1. PD controller type under AD

A system with non-nominal parameters is obtained when Eq. 47 is feedback controlled with the nominal gain matrix of the PD controller (Eq.35). The transfer function achieved is in the following equation:

$$Z(s) = \frac{\frac{Z_{ref}(s)\alpha_0 a^2}{\alpha} + \frac{V_D(s)}{\alpha}}{s^2 + s\frac{2a\alpha_0 + \beta - \beta_0}{\alpha} + \frac{\alpha_0 a^2 + \gamma_0 - \gamma}{\alpha}} \tag{48}$$

By applying the final value theorem under the hypothesis of a step funcion as a perturbation, a step input as a reference, and by considering that the difference between the real value and the nominal value of the compressibility coefficient is null, we obtain that the time response in steady state is different from the output signal:

$$\lim_{t\to\infty} z(t) = \lim_{s\to 0} s \cdot Z(s) = \lim_{s\to 0} \frac{\frac{Z_{ref}(s)\alpha_0 a^2}{\alpha} + \frac{\Delta V_D(s)}{\alpha}}{s^2 + s\frac{2a\alpha_0 + \beta - \beta_0}{\alpha} + \frac{\alpha_0 a^2 + \gamma_0 - \gamma}{\alpha}} \neq Z_{ref} \tag{49}$$

The system is strongly dependent not only on the non-correspondence with the non-nominal values of modeling, but also on the quantification of the external perturbations. The use of PD controllers is, therefore, ruled out.

7.2. I-PD controller type under AD

In order to analyze the behavior of this controller under conditions of external disturbances, the transfer function will be obtained in a similar way to that which occurred for the previous controller, but in this case, the gain matrix that is used corresponds to Eq. 31.

$$Z(s) = \frac{\frac{4a^3\alpha_0 Z_{ref}(s)}{\alpha}}{s^3 + s^2\left(\frac{5a\alpha_0+\beta-\beta_0}{\alpha}\right) + s\left(\frac{8a\alpha_0+\gamma_0-\gamma}{\alpha}\right) + 4a^3\frac{\alpha_0}{\alpha}} + \frac{\frac{s\Delta V_D(s)}{\alpha}}{s^3 + s^2\left(\frac{5a\alpha_0+\beta-\beta_0}{\alpha}\right) + s\left(\frac{8a\alpha_0+\gamma_0-\gamma}{\alpha}\right) + 4a^3\frac{\alpha_0}{\alpha}} \tag{50}$$

The final value theorem is applied under the hypothesis that both the disturbance and the reference signal are also step-based input signals:

$$\lim_{t\to\infty} z(t) = \lim_{s\to\ 0} s \cdot Z(s) = \lim_{s\to\ 0} \frac{\frac{4a^3\alpha_0 Z_{ref}(s)}{\alpha} + \frac{s\Delta V_D(s)}{\alpha}}{s^3 + s^2\left(\frac{5a\alpha_0+\beta-\beta_0}{\alpha}\right) + s\left(\frac{8a\alpha_0+\gamma_0-\gamma}{\alpha}\right) + 4a^3\frac{\alpha_0}{\alpha}} = Z_{ref} \tag{51}$$

The disturbance produced by the loss of buoyancy that the device undergoes close to the surface can be canceled by the controller. To reduce the effort of this controller, the control signals responsible for minimizing the effects of unmodeled disturbances can be generated in a similar way to that carried out with simpler controllers of manipulator robots, which have to cancel the nonlinear effect of gravity. The proposed control signal is the same as in Eq.26, but an estimate (subindex $_e$) of the compensation of the loss of buoyancy, $V_{Bouy_e}[z(t)]$, has been added, which is Laplace transformable as $\mathcal{L}[V_{Bouy_e}[z(t)]] = V_{Bouy_e}(s)$ and its $\lim_{s\to\ 0} V_{Bouy_e}(s) = V_{Bouy_e}$.

$$\Delta V_u = k_{\epsilon 0} \cdot x_\epsilon + \mathbf{K}_{FE0} \cdot \mathbf{x} + V_{Bouy_e} \tag{52}$$

This compensation is not considered perfect, and it is for this reason that in this case, the additive disturbance, $\widehat{\Delta V}_D$ is the difference between the real additive disturbance and the computed loss of buoyancy ($\widehat{\Delta V}_D(s) = \Delta V_D(s) - V_{Bouy_e}(s)$). The transfer function is:

$$Z(s) = \frac{\frac{4a^3\alpha_0 Z_{ref}(s)}{\alpha} + \frac{s\widehat{\Delta V}_D(s)}{\alpha}}{s^3 + s^2\left(\frac{5a\alpha_0+\beta-\beta_0}{\alpha}\right) + s\left(\frac{8a\alpha_0+\gamma_0-\gamma}{\alpha}\right) + 4a^3\frac{\alpha_0}{\alpha}} \tag{53}$$

By applying the final value theorem when the reference and the disturbance are a step input signals:

$$\lim_{t\to\infty} z(t) = \lim_{s\to\ 0} s\cdot Z(s) = \lim_{s\to\ 0} \frac{\frac{4a^3\alpha_0 Z_{ref}(s)}{\alpha} + \frac{s\widehat{\Delta V}_D(s)}{\alpha}}{s^3 + s^2\left(\frac{5a\alpha_0+\beta-\beta_0}{\alpha}\right) + s\left(\frac{8a\alpha_0+\gamma_0-\gamma}{\alpha}\right) + 4a^3\frac{\alpha_0}{\alpha}} = Z_{ref} \tag{54}$$

The time response of the system is, therefore, in the steady state near the free surface and while the actuators can compensate for the buoyancy force, the time response will be faster only if the difference in the losses in buoyancy have to be compensated. This result can be extrapolated to any other additive disturbance to the control signal.

The desired behavior for non-nominal values and in the presence of external disturbances is provided by the I-PD controller, as can be seen in the simulations (Figs. 25-28), which correspond to the time responses of the emersion maneuvers with linear trajectories of order 6 [54] of different times, denominated as ΔT_{EM} from 600 to 1200s, in the presence of several steps based on external disturbances, $\Delta F = \Delta V \cdot \rho_w \cdot g$.

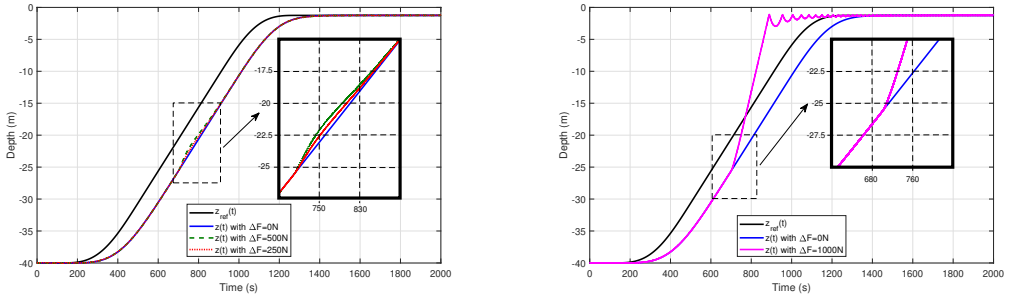

Figure 25: $\Delta T_{EM} = 1200s$ and time response of the device when ΔF is applied at 700s.

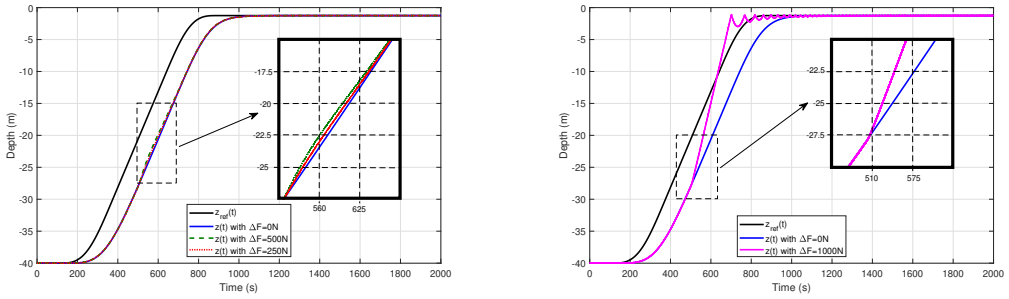

Figure 26: $\Delta T_{EM} = 800s$ and time response of the device when ΔF is applied at 500s.

The controller is capable of canceling external disturbances as long as it does not exceed the capacity of the actuators, as can be seen in simulations on the left. However, in the simulations on the right, the system loses control owing to the maximum compensation capacity of the actuators. In this case, the actuator is not able to compensate the external disturbance. In other words, the control system does not work. The similarity of the time response shown in the right-hand simulations can be verified using the time response presented in [15].

8. Complete emersion/maintenance/immersion maneuver responses

Having analyzed the system with I-PD controller behavior when it performs well, even with greater α and β variations and strongly force disturbances when tracking trajectories, in this section, a complete emersion/time of maintenance task/immersion sequence is discussed.

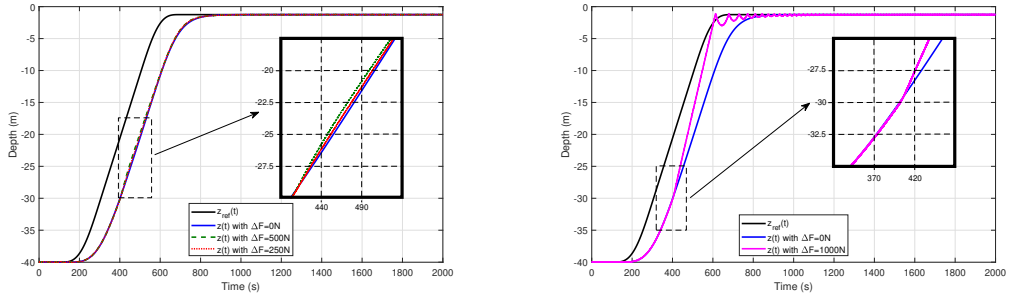

Figure 27: $\Delta T_{EM} = 600s$ and time response of the device when ΔF is applied at $400s$.

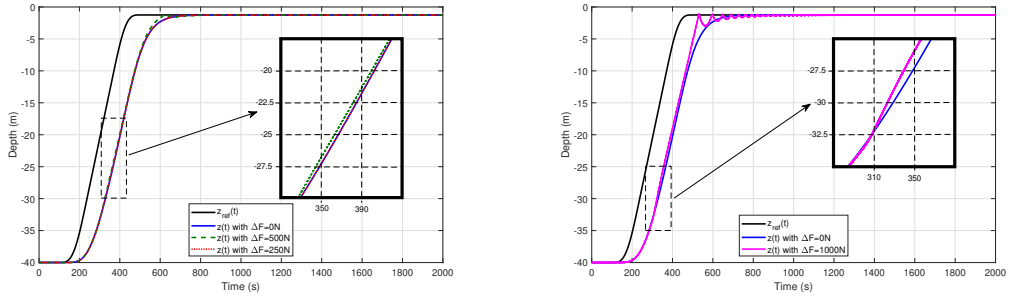

Figure 28: $\Delta T_{EM} = 600s$ and time response of the device when ΔF is applied at $300s$.

The use of the references $z_{ref} > -R$, where R denotes the radius of the cylinder, is strongly discouraged owing to the limitation of the actuators responsible for the V_{Bouy} compensation. Since the temporary interval when the device remains in the neighborhood of the free surface of the sea can be very long with respect to the emersion and immersion times, an intermediate time interval has been included between these motion time intervals for the complete simulations of the maneuvers. This intermediate interval has been deliberately reduced in time only for simulation purposes, as can be seen below.

This is the main reason why, during the intermediate interval when the device has been emerged, we propose:

- The disconnection of the closed loop control.
- A reduction in draught by means of a central ballast tank (CBT), not used for the closed loop control, which is managed by the use of water pumps (details in [53])

Once the maintenance tasks have been completed, the CBT is again flooded before the immersion maneuver is started synchronously with the connection of the closed loop control.

The complete procedure of emersion and immersion is, therefore, proposed, which is divided into the following three stages:

- Stage Emersion (EM): Closed loop motion of the device between the instants $t_1 = 100s$ and $t_2 = 1000s$, with a linear reference with order 6 polynomial blends [54] from the nominal depth, $z_{DW} = -40m$ to a depth of $z_{UP} = -1.25m$ in $600s$, then a constant reference at $z_{UP} = -1.25m$ until t_2, signifying that the device does not have any interaction with the free surface.
- Stage Maintenance tasks (MA): Time interval between t_2 and $t_3 = 1600s$ (It can be increased). These tasks time is decomposed into three substages:

- MA-1: Disconnection of the closed loop control at t_2, then emptying the CBT (its capacity is $0,3m^3$) between the instants t_2 and $t_{21} = 1100s$.
- MA-2: Maintenance tasks between instants t_{21} and $t_{22} = 1500s$ (whose time can be increased).
- MA-3: Flooding of the CBT between t_{22} and t_3. Once full, the closed control system is again connected at t_3.

- Stage Immersion (IM): Closed loop motion of the device between t_3 and $t_4 = 2500s$, with an identical linear reference, but in this case from depth $z_{UP} = -1.25m$ to its nominal depth $z_{DW} = -40m$. Then the whole process ends.

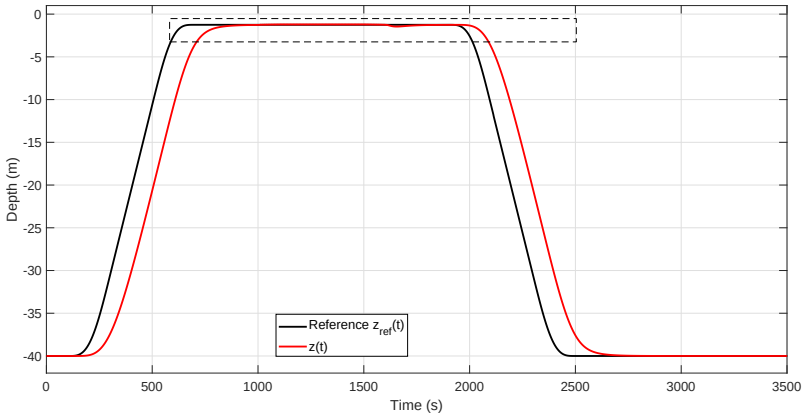

Figure 29: Time response for proposed maneuver and $CBT = 0.3m^3$

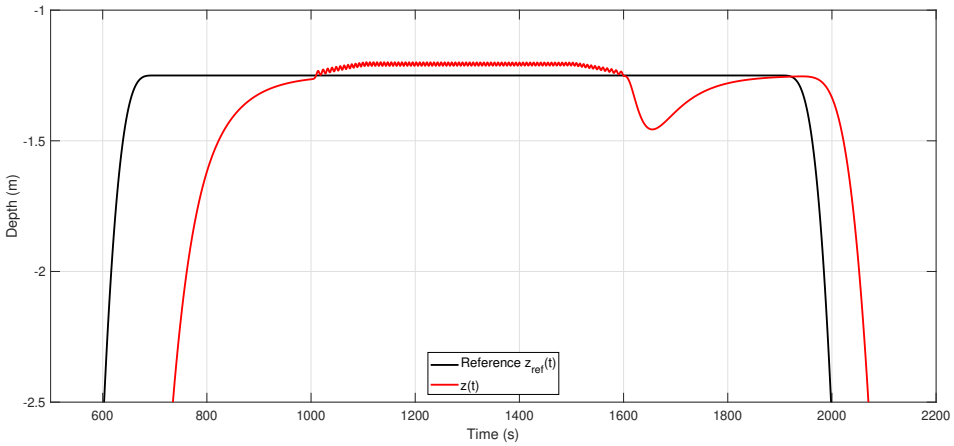

Figure 30: Time response for proposed maneuver and $CBT = 0.3m^3$(Zoom)

Fig. 29 shows the time response of the device for the maneuvers described, while Fig. 30 presents the zoom of the time interval between the instants $500s \leq t < 2200s$ in the neighborhood of the free surface, in which it can be noted that there is a reduction of the draught of the device when the CBT is fully emptied and when it is filled again. Moreover, the device sinks by a further $0.2m$, until the controller is able to correct this variation. This kind of behavior with respect to the immersion response was already known by submarine commanders as far back as 1915 [55], [56].

In order to avoid a situation in which the device suddenly descends and then rises to the surface again, we propose to slightly modify the IM Stage into two substages:

- IM-1: The reference signal becomes a step function from $z_{UP} = -1.25m$ to an intermediate depth $z_{IN} = -2m$, which is maintained until $t_{31} = 1900s$.
- IM-2: Immersion with a linear reference of the device between t_{31} and t_4, from $z_{IN} = -2m$ to its nominal depth $z_{DW} = -40m$.

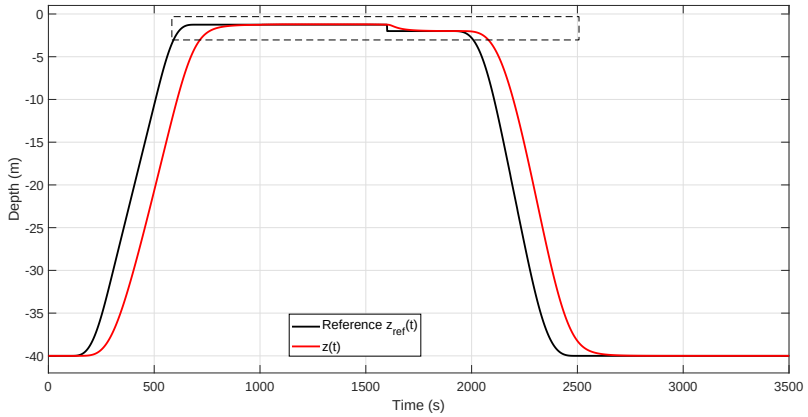

Figure 31: Time response for proposed maneuver with step reference and $CBT = 0.3m^3$

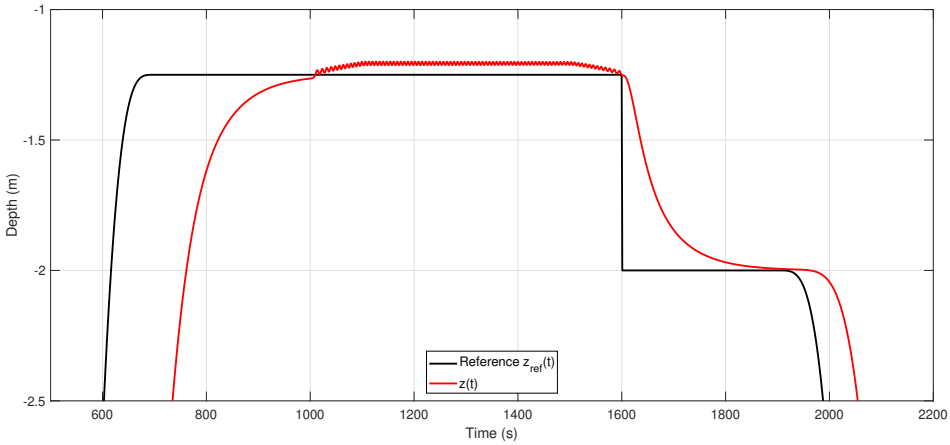

Figure 32: Time response for proposed maneuver with step reference and $CBT = 0.3m^3$ (Zoom)

The time response of the system for the new reference signal can be seen in Fig. 31, while the zoom is shown in Fig. 32, which illustrates a gentler descent of the device than in the previous simulation.

The time response for the same reference is depicted in Fig. 33, but when the capacity of the CBT has been increased to $3m^3$ rather than $0.3m^3$. In this case, the CBT is emptied between t_2 and $t_{21} = 1200s$, and is flooded between $t_{22} = 1400s$ and t_3. The device reaches a greater depth than that desired and goes back up to $z_{IN} = -2m$. As can be noted in Fig. 34, the device does not descend as gently as in the previous simulation.

A new and final control strategy for Stage IM-1 is proposed, which consist of using the linear reference type with different time intervals, denoted as ΔT_{St}, when the device has to descend from z_{UP} to z_{IN} instead of a step reference. The different time responses for these reference signals, but when the device is kept at z_{IN} for longer, denoted as $\Delta T_{waiting}$, can be observed in Fig. 35. The extra time, $\Delta T_{waiting}$, is used for the stabilization of the device at the desired intermediate depth z_{IN}.

The zoom shown in Fig. 36, is now shown between the interval $500s \leq t < 2500s$, and it will be noted that the control system is not able to follow the desired references. The lowering of the device

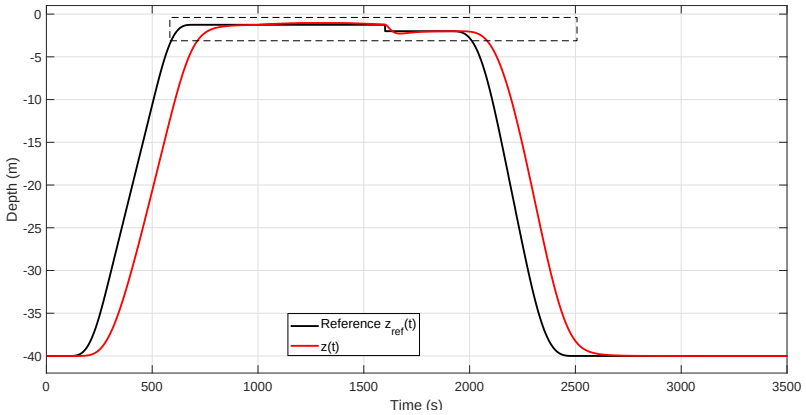

Figure 33: Time response for proposed maneuver with step reference and $CBT = 3m^3$

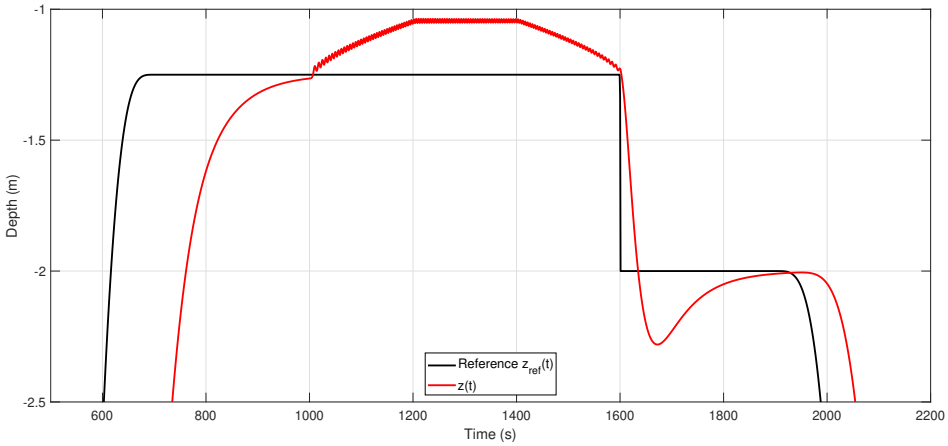

Figure 34: Time response for proposed maneuver with step reference and $CBT = 3m^3$ (Zoom)

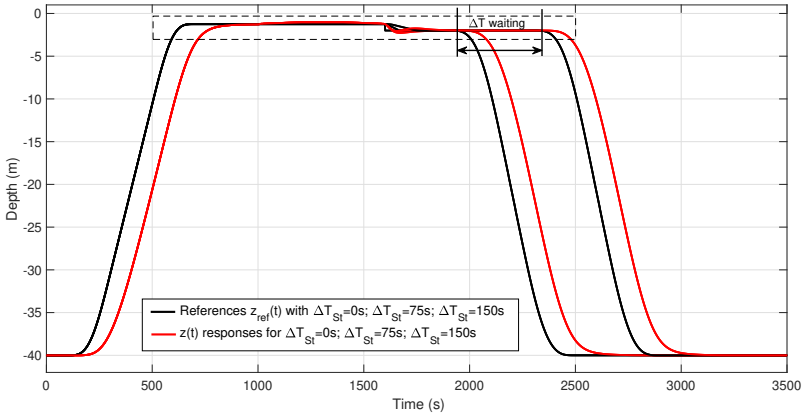

Figure 35: Time response for proposed maneuver with different ΔT_{St} and $CBT = 3m^3$

coincides for all reference signals to the neighborhood of the instant $t = 1650s$ because of the instability associated with submerged bodies and the transition from open loop to closed loop dynamics taken at t_3. From this instant, the best dynamics behavior is observed when the transition reference from z_{UP} to z_{IN} is planned with with $\Delta T_{St} = 75s$, but this conclusion is strongly dependent on the speed of the actuators, the capacity of the control ballast tanks, the water pumps system performance in the CBT,

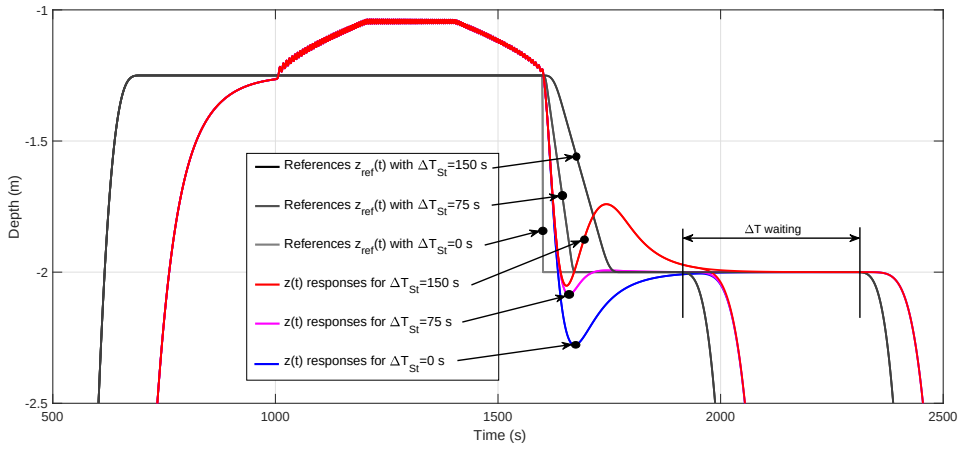

Figure 36: Time response for proposed maneuver with different ΔT_{St} and $CBT = 3m^3$ (Zoom)

and the environmental disturbances as waves from the sea, among others.

9. Experimental Validation

The dynamic model in open-loop was originally proposed and experimentally validated in [15]. This research work, therefore, shows a large number of experiments that were carried out to validate the various control algorithms proposed in this research and which took place in the calm water basin located in the E.T.S. Ingenieros Navales at the Universidad Politécnica de Madrid [57]. The following constraints were addressed in the design of the proposed prototype (resumed from [15]):

- The dimensions of the prototype had to be appropriate for the dimensions of the model basin, which is 2.20 m in depth, 3.80 m in width and 100 m in length.
- The prototype designed had a cylinder-based form with a three-bladed passive rotor at the bow and a semi-sphere at the stern.
- The prototype was designed to be modular in order to facilitate interchangeability, future expansion and easy assembly/disassembly.
- The prototype had to be highly instrumented in order to permit the study of its dynamics, the implementation of different feedback control systems and data acquisition for the purpose of further analysis.
- There had to be on-board distributed instrumentation so as to minimize the presence of external wires: only a 24VDC supply and an Industrial Ethernet/EtherCAT cable are used.

Table 2 shows the principal dimensions of the prototype in accordance with the design aims. Subscript 0 is used to denote nominal values and Figure 37 provides a general view of the prototype used, which has the three-bladed passive rotor with a semi-sphere hub at the bow and a transparent semi-sphere at the stern. These are located in this way in order to minimize non-linear hydrodynamic effects, such as turbulence, vortices, etc. when the cylinder is moving. Both the hub and the semi-sphere were perforated at several points in order to enable water to be trapped between the flat end faces of the cylinder and the inner side of each semi-sphere. The overall length of the prototype is 0.810 m, whereas the term ”length” in Table 2 refers to cylinder length. The three-blade rotor was specially manufactured for this prototype using polylactic acid (PLA) material and a 3D printer, giving it a density of 1000 kg $\cdot$ m^{-3}, while the semi-sphere was made of methacrylate.

Magnitude	Nominal Value	Units
L	0.608	m
R	0.100	m
m	18.7	kg
V_0	0.191	m^3
ν	79.4	$N \cdot s^2 \cdot m^{-2}$
γ_0	2.0e-8	m^2
g	9.81	$m \cdot s^{-2}$
ρ_w	1000	$kg \cdot m^{-3}$

Table 2: Nominal parameter values

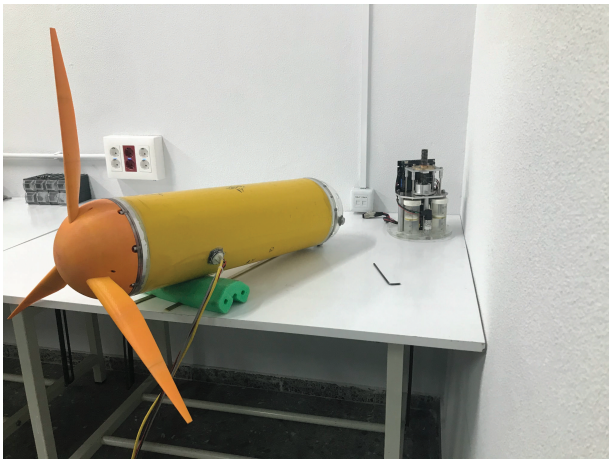

Figure 37: General View of the experimental laboratory prototype used in the experiments.

Two actuator sets are coupled on both ends of the cylinder in order to provide the platform with buoyancy control, which is achieved by changing the volume of four small controlled pistons attached to each actuator. Incremental changes in volume are achieved by means of longitudinal piston displacements. The associated servo-system is composed of a Maxon RE40 DCmotor (⌀ 40 mm) with 150 Watt Graphite Brushes, a gear reduction and a trapezoidal spindle/nut of 8 mm per lap in order to convert the rotational motion of the gear shaft into linear piston displacement. This system is responsible for producing half of $\Delta V_u(t)$, up to ± 0.400 liters each. The position of the four pistons is controlled using a Maxon EPOS2 and an embedded encoder.

Two differential pressure sensors (DPF) E13-VF with a fullscale absolute pressure of 1.6 bars are used as primary depth-z sensors. They are placed on each of the flat faces of the cylinder. Each sensor provides a full scale 0..10 V output signal. Another external and identical sensor is used to discount the atmospheric pressure for calibration with a water depth of -z. Because the same prototype can be used to obtain two degrees-of-freedom motions (depth and orientation), a Microstrain 3DM-GX4-15 Inertial Measurement Unit (IMU), located inside with its X-axis aligned with the main axis of the cylinder, is used for orientation measurements.

The device is controlled using an embedded Beckhoff CX2030 computer with 2GB RAM Memory, two independent Gbit Ethernet interfaces, four USB 2.0 interfaces and a DVI-I interface, which runs under a Microsoft Embedded Windows Operative system. This is placed outside the prototype and is connected via Ethernet to a Personal Computer with Microsoft Windows and the TwinCAT3 PLC/C++ programming module. This Personal Computer is used with both the host and the development unit. The Graphical User Interface and the programming environment are handled by Microsoft Visual Studio.

Finally, a set of modular and distributed instrumentation systems is located inside the prototype. This set consists of a Beckhoff EK1814 EtherCAT Coupler with integrated digital inputs/outputs and an EtherCAT connection with the outside CX2030 computer. This coupler has been extended using the following three modules: i) an EL6002 serial interface module that enables communication with the MicrostrainIMU via RS232; ii) an EL6751 CANOpen master terminal module that is responsible for handling the communications with the MAXON EPOS, and iii) the EL3102 2-channel analog input terminal -10...+10V module, which is used to obtain the voltage signals from the pressure sensors. All these modules are connected to the outside CX2030 computer via the EK1814 coupler and EtherCAT connection. Figure 38 shows a general scheme of the hardware architecture. The umbilical connection from the prototype to the outside is formed solely of an EtherCAT wire and a 24 VDC power supply line. The number of actuator sets and similar cylinders can be increased by using the same architecture with only an EtherCAT Extension and a 24 VDC power supply, which is omitted from this figure.

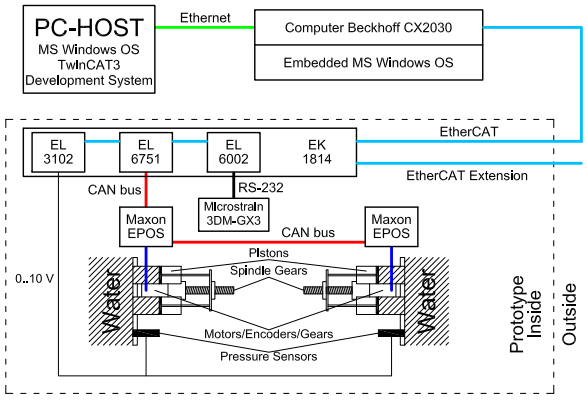

Figure 38: General Hardware Architecture

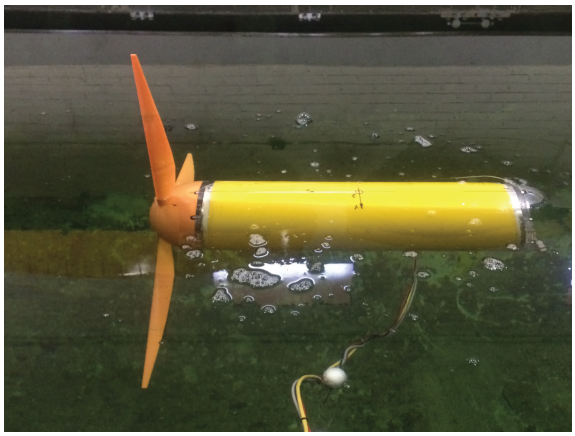

Figure 39: Prototype during MA stage

In order to validate both the proposed dynamic control and the procedure depicted in Section 8, the performance of the proposed emersion/immersion strategy was verified by carrying out experimental trials in the calm water basin located in the E.T.S. Ingenieros Navales at the Universidad Politécnica de Madrid. The photograph in Figure 39 shows an instant of the motion of the prototype during the Maintenance (MA) stage. Note the appearance of the umbilical wire in the lower half of this photograph, together with the reflection of one of the lighting devices located on the roof and deformed by the water.

Figure 40 depicts both the reference signal and the z-response for a complete sequence of emersion/immersion maneuver. Bearing in mind the notation illustrated in Section 7, linear trajectories with 6th order polynomic blends were used as closed loop references. The EM stage is executed between $t_1 = 20$ s and $t_2 = 60$ s with $z_{DW} = -1.780$ m and $z_{UP} = -0.125$ m in 35 s respectively; the MA stage took place between t_2 and $t_3 = 80$ s, when the closed loop was disconnected and the actuators provided 3.9 N of extra force in open loop that emulated the CBT, which did not exist in the prototype (neutral buoyancy was obtained with the actuator sets, located at 50% of their linear displacement ranges). The last IM stage was executed in closed loop with a constant reference at $z_{IN} = -0.200$ m during 25 s with a $\Delta T_{St} = 2.3$ s in the first sub-stage, and then, with a similar linear trajectory as a reference from z_{IN} to z_{DW} at $t_4 = 140$ s and with a duration of 35 s was used as a closed loop reference for the second sub-stage of the Immersion Maneuver (IM) stage. An I-PD controller that was tuned for obtaining a closed loop characteristic polynomial with a parameter of a = 0.05 rad/s (see equation 32) was implemented in accordance to equation 26.

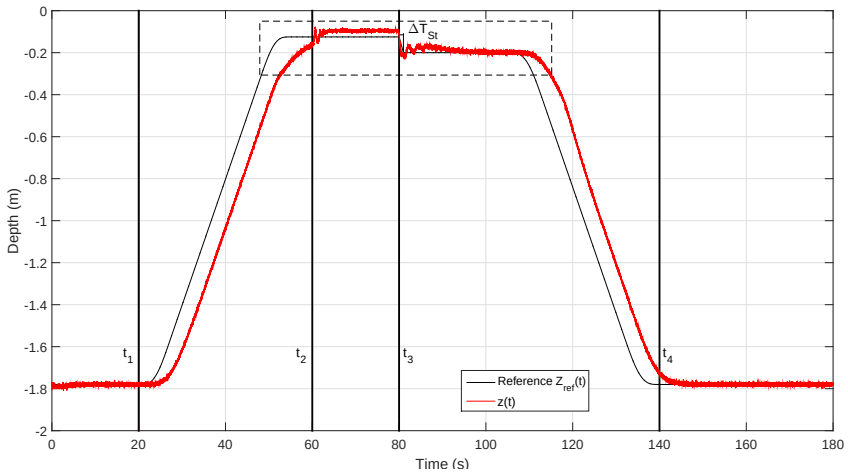

Figure 40: Time Response of the complete emersion/inmersion maneuver.

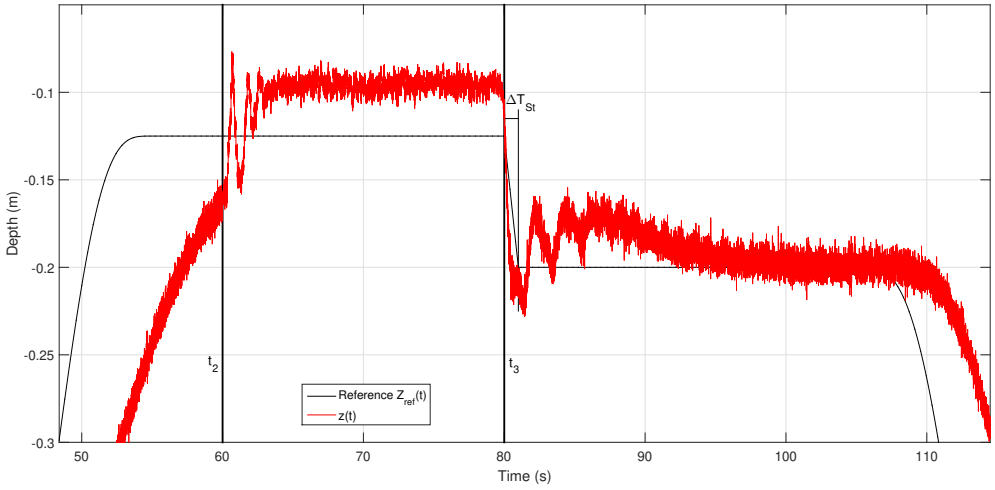

Figure 41: Time Response of the complete emersion/inmersion maneuver (Zoom).

It was easily verified that the proposed closed/open loop strategy for a complete closed loop emersion/immersion maneuver with an intermediate MA time in open loop has a very good fit with the

expected simulation results. In a similar manner to that which occurred in Figures 30, 32 and 34, both the closed loop reference and the time response of the depth-z measurement have been enlarged in Figure 41 so as to better illustrate that there is a very high correspondence with the aforementioned numerical simulations shown in the above previous figures. In this experiment, the mean value of the depth during the MA stage was $z = -0.089$ m.

10. Conclusions

Tidal energy is one of the most promising renewable energies thanks to its enormous potential for electricity production and its predictable character. Although the tidal energy industry has only just begun to demonstrate full-scale devices and device arrays, the nascent status of these technologies signifies that they have not yet obtained a sufficient level of reliability, feasibility and survivability to be marketable when compared to other renewable technologies. In order to ensure the future viability of these technologies and a sustained commercially competitive cost of energy, important efforts have to be made in order to reduce their associated costs. One of the principal keys for the future success of these technologies is the provision of a secure infrastructure (grid access, supply chain, maintenance service, etc.). This paper is focused on the development of new forms of maintenance services and, in particular, on the study of ease-of-installation and ease-of-maintenance systems (by means of the design of new control systems that allow the automatic change of orientation/depth of the TEC) for gravity-based first generation TECs in order to reduce their maintenance intervals (and consequently their costs) and optimize the harnessing of the energy resource.

A very simple dynamic model has been obtained, which has allowed the design of the control systems to be carried out from the linearization of the proposed dynamic model, after which the behavior of the device in closed-loop has been studied by means of PD and I-PD controllers. The results obtained from the numerical simulations verify that the closed-loop system with the I-PD control scheme provides a better desired transient response, null errors in steady-state between the reference input and the simulated response of the device, along with the excellent behavior of the system in the presence of parametric changes and non-modeled external disturbances. Furthermore, temporary references have been generated in order to be used as command signals to perform a complete emersion and immersion maneuver including strong disturbances, which could occur in a real device, and demonstrating that it is feasible to control the system even under the effect of these perturbations, thus guaranteeing its viability. The proposed control system together with the performance of the emersion/immersion strategy have been demonstrated by means of numerical simulations and experimental trials. The convincing experimental results validate the effectiveness of the controller and the emersion/immersion strategy, revealing that they successfully deal with non-nominal conditions and in the presence of strong external disturbances. Finally, it is important to highlight that the control system developed in this work is of a general nature and its applicability can be extended not only to the second generation tidal energy converters, but also to any device that has to perform emersion/immersion maneuvers, thus providing great versatility to this control system.

Acknowledgements

This research has been partially supported by the Spanish Ministerio de Economía y Competitividad and Ministerio de Ciencia, Innovación y Universidades under Research Grants DPI2014-53499-R and PID2019-104995RB-I00.

References

[1] Vicinanza, D., Contestabile, P., Nørgaard, J., Lykke Andersen, T., 2014. Innovative rubble mound breakwaters for overtopping wave energy conversion. *Coast. Eng.*, vol. 88, 154–170.

[2] Stokes, C., Beaumont, E., Russel, P., Greaves, D., 2014. Anticipated coastal impacts: what water-users think of marine renewables and why. *Ocean Coast. Manag.*, vol. 99, 63–71.

[3] Dalir, F., Motlagh, M.S., Ashrafi, K., 2018. A dynamic quasi comprehensive model for determining the carbon footprint of fossil fuel electricity: a case study of Iran. *J. Clean. Prod.*, vol. 188, 362–370.

[4] Younesian D. and Alam M.-R., Multi-stable mechanisms for high-efficiency and broadband ocean wave energy harvesting. *Applied Energy*, vol. 197, pp. 292–302, 2017.

[5] Amrollahi M.H. and Taghi Bathaee S.M., Techno-economic optimization of hybrid photovoltaic/wind generation together with energy storage system in a stand-alone micro-grid subjected to demand response. *Applied Energy*, vol. 202, pp. 66–77, 2017.

[6] Facci A.L., Cigolotti V., Jannelli E., Ubertini S., Technical and economic assessment of a SOFC-based energy system for combined cooling, heating and power. *Applied Energy*, vol. 192, pp. 563–574, 2017.

[7] Alashkar A. and Gadalla M., Thermo-economic analysis of an integrated solar power generation system using nano fluids. *Applied Energy*, vol. 191, pp. 469–491, 2017.

[8] A Clean Planet for all. A European strategic long-term vision for a prosperous, modern, competitive and climate neutral economy. *Communication from the Commission to the European Parliament, the European Council, the Council, the European Economic and Social Commitee, the Commitee of the Regions and the European Investment Bank*, 28 November 2018, COM(2018) 773 final.

[9] Offshore wind energy: action needed to deliver on the energy policy objectives for 2020 and beyond. *Communication from the commission to the European parliament, the council, the European economic and social committee and the committee of the regions.*, 12.12.2008, COM(2008), 768 final/2.

[10] Foteinis, S., Hancock, J., Mazarakis, N., Tsoutsos, T., Synolakis. C.E., A comparative analysis of wave power in the nearshore by WAM estimates and in-situ (AWAC) measurements. The case study of Varkiza, Athens, Greece. *Energy*, 138, 500–508, 2017.

[11] Zarzuelo, C., López-Ruiz, A., Ortega-Sánchez M., Impact of human interventions on tidal stream power: the case of Cádiz Bay. *Energy*, 145, 88–104, 2018.

[12] A strategy for smart, sustainable and inclusive growth. *Communication from the Commission - Europe 2020*, 03.03.2010, COM(2010), 2010.

[13] Rodríguez-Delgado, C., Bergillos R.J., Iglesias, G., Dual wave farms for energy production and coastal protection under sea level rise. *Energy*, 222, 364–372, 2016.

[14] Vázquez, A.; Iglesias, G., Capital costs in tidal stream energy projects – A spatial approach. *Energy*, 107, 215–226, 2016.

[15] Somolinos, J.A.; López, A.; Núñez, L.R.; Morales, R. Dynamic model and experimental validation for the control of emersion maneuvers of devices for marine currents harnessing. *Renew. Energy*, *107*, 333–345, 2017.

[16] Magagna D., MacGillivray A., Jeffrey H., Hanmer C., Raventos A., Badcock-Broe A. and Tzimas E., Wave and Tidal Energy Strategic Technology Agenda. *SI Ocean*, 2014.

[17] Arent D.J., Wise A. and Gelman R., The status and prospects of renewable energy for combating global warming. In *Energy Economics*, vol.33, pp. 584–593, 2011.

[18] Jeffrey H., Jay B. and Winskel M., Accelerating the development of marine energy: exploring the prospects, benefits and challenges. In *Technological Forecasting and Social Change*, vol.80, pp. 1306–1316, 2013.

[19] European Commission, 2014. Blue Energy Action needed to deliver on the potential of ocean energy in European seas and oceans by 2020 and beyond. COM/2014/08. Avaiable online: `http://eur-lex.europa.eu/legal-content/EN/TXT/?uri=CELEX:52014DC0008` (accessed on 07/09/2019).

[20] Andritz Hydro Hammerfest. How it works. Available online: `https://www.andritz.com/hydro-en/hydronews/27/hy-news-27-03-tidal-energy-hydro` (accessed on 05/09/2019).

[21] Alstom Tidal Turbines Web Page. Available online: `http://alstomenergy.gepower.com/products-services/product-catalogue/power-generation/renewable-energy/ocean-energy/tidal-energy/tidal-power/index.html` (accessed on 05/09/2019).

[22] Verdant Power. Kinetic Hydropower System (KHPS), 2006. Available online: `http://www.verdantpower.com/kinetic-hydropower-system.html` (accessed on 05/09/2019).

[23] Segura, E.; Morales, R.; Somolinos, J.A.; López, A. Techno-economic challenges of tidal energy conversion systems: Current status and trends. *Renew. Sustain. Energy Rev.*, *77*, 536–550, 2017.

[24] ICES Scientific Reports. 1:6. 95 pp. `http://doi.org/10.17895/ices.pub.4914` (accessed on 07 June 2020).

[25] REN21. 2019. *Renewables 2019 Global Status Report*. (Paris: REN21 Secretariat). ISBN 978-3-9818911-7-1

[26] Simec Atlantis Energy Web Page. Available online: `https://simecatlantis.com/projects/meygen/` (accessed on 07 June 2020).

[27] Morales R., Fernández L., Segura E. and Somolinos J.A., Maintenance maneuver automation for an adapted cyclindrical shape TEC. *Energies*, vol. 9(9), pp. 746, 2016.

[28] Somolinos J.A., López A., Portilla M.P. and Morales R., Dynamic Model and Control of a New Underwater Three-Degree-of-Freedom Tidal Energy Converter. *Mathematical Problems in Engineering*, Article ID 948048, 2015. doi:*http://dx.doi.org/10.1155/2015/948048*.

[29] Portilla M.P., López A., Somolinos J.A., Morales R. Modelado dinámico y control de un dispositivo sumergido provisto de actuadores hidrostáticos. *Revista Iberoamericana de Automática e Informática Industrial*, 15, 12–23, 2018.

[30] Thies P.R., Johanning L. and Smith G.H., Towards component reliability testing for marine energy converters. *Ocean Engineering*, vol. 38, pp. 360–370, 2011.

[31] Walker J.M., Flack K.A., Lust E.E., Schultz M.P., Luznik L., Experimental and numerical studies of blade roughness and fouling on marine current turbine performance. *Renewable Energy*, vol. 66, pp. 257–267, 2014.

[32] Segura E., Morales R. and Somolinos J.A., Cost assessment methodology and economic viability of tidal energy projects. *Energies*, vol. 10(11), 1806; doi:10.3390/en10111806, 2017.

[33] Segura E., Morales R. and Somolinos J.A., A strategic analysis of tidal current energy conversion systems in the European Union. *Applied Energy*, vol. 212, pp. 527–551, 2018.

[34] Segura E., Morales R. and Somolinos J.A., Increasing the Competitiveness of Tidal Systems by Means of the Improvement of Installation and Maintenance Maneuvers in First Generation Tidal Energy Converters – An Economic Argumentation. *Energies*, vol. 12, 2464; doi:10.3390/en12132464, 2019.

[35] Segura E., Morales R. and Somolinos J.A., Influence of Automated Maneuvers on the Economic Feasibility of Tidal Energy Farms. *Sustainability*, vol. 11, 5965; doi:10.3390/su11215965, 2019.

[36] ABR Company Ltd. International Tug & OSV, Incorporating Salvage News, 2017. Available online: `https://www.tugandosv.com/about_the_magazine.php` (accessed on 2 April 2020).

[37] Voith. Tidal Current Power Stations. Available online: `http://voith.com/en/productsservices/hydro-power/ocean-energies/tidal-current-power-stations--591.html` (accessed on 2 April 2020).

[38] Sánchez, G. Diseño de un Dispositivo Para el Aprovechamiento de la Energía de las Corrientes (DAEC) y su Integración en un Parque Marino. Master's Thesis, Escuela Técnica Superior de Ingenieros Navales Universidad Politécnica de Madrid (ETSIN-UPM), Madrid, Spain, 2014.

[39] BVG Associates. *A Guide to an Offshore Wind Farm*; The Crown Estate: London, UK, 2010.

[40] Riviera Maritime Media, Ltd. Offshore Wind Journal 4th Quarter 2014. 2014. Available online: `http://free.yudu.com/item/embedded_reader/2557767/Offshore-Wind-Journal-4th-Quarter-2014` (accessed on 2 April 2020).

[41] Riviera Maritime Media, Ltd. OSJ Offshore Support Journal. 2015. Available online: `http://www.osjonline.com/.Consultadoel27/01/2015` (accessed on 2 April 2020).

[42] TradeWinds. TradeWinds Weekly January 2015. 2015. Available online: `http://www.tradewindsnews.com/` (accessed on 2 April 2020).

[43] Khan, J.; Bhuyan, G.S. Ocean Energy Global Technology, Development Status. Final Technical Report. IEA-OES Document No T0104. 2015. 2009. Available online: `http://www.ocean-energysystems.org/documents/30692_annex_1_doc_t0104.pdf/` (accessed on 26 August 2019).

[44] Fernández, L.; Segura, E.; Portilla, M.P.; Morales, R.; Somolinos, J.A. Dynamic model and nonlinear control for a two degrees of freedom first generation tidal energy converter. *IFAC-PapersOnLine* **2016**, *49–23*, 373–379.

[45] IEC-TC214. Technical specification: Marine energy. Wave, tidal and other water current converters. Part 1: Terminology, *IEC/TS 62600-1 Ed. International Electrotechnic Commision. Ginebra, Switzerland*, 2011.

[46] Nise N.S., Control Systems Engineering. *John Wiley & Sons Inc.*, ISBN 978-1119590132, 2019.

[47] Dorf R.C., Modern Control Systems, Global Edition. *Pearson Education Limited*, 13th Ed., ISBN 978-1292152974, 2016.

[48] Houpis C.H. and Sheldon S.N., Linear Control System Analysis and Design with MATLAB. *CRC Press*, ISBN 9781466504264, 2013.

[49] Lurie B.J. and Enright P., Classical Feedback Control: With MATLAB and Simulink, 2nd Ed. *CRC Press*, ISBN 9781439860175, 2011.

[50] Dutton K., Thompson S. and Barraclough B., The Art of Control Engineering, First Ed. *Prentice Hall*, ISBN 978-0201175455, 1997.

[51] Goodwin G.C., Graebe S.F. and Salgado M.E., Control System Design *Pearson*, ISBN 978-0139586538, 2000.

[52] Ogata K., Modern Control Engineering, Fifth Edition. *Prentice Hall*, ISBN 978-0136156734, 2009.

[53] Espín M., Modelado Dinámico y Control de Maniobras de Dispositivos Submarinos. *Ph.D. Thesis. ETSIN-UPM*, 2015.

[54] Perumaal, S.S.;Jawahar, N., Automated trajectory planner of industrial robot for pick-and-place task. *International Journal of Advanced Robotic Systems*, vol. 10(2), pp. 1–17,2013.

[55] Captain D. Manuel Pasquín. Maniobras de inmersión de los sumergibles. *Revista de la Marina*, pp. 131–149, 1915.

[56] Lieutenant C.N: Hinkamp. Submarinos. *Revista de la Marina*, pp. 383–393, 1915.

[57] Model Basin Research Group. Section Facilities and Equipments. `http://www.http://canal.etsin.upm.es/?lang=en` (accessed on 07 April 2020).